Electronic supplementary information

Manipulating regioselectivity of an epoxide hydrolase for single enzymatic synthesis of (*R*)-1,2-diols from racemic epoxides

Die Hu,‡[a] Xun-Cheng Zong,‡[b] Feng Xue,‡[c] Chuang Li,[b] Bo-Chun Hu[b] and Min-Chen Wu*[a]

[a] *Wuxi School of Medicine,* Jiangnan University, Wuxi, 214122, China.

[b] *Key Laboratory of Carbohydrate Chemistry and Biotechnology, Ministry of Education, School of Biotechnology, Jiangnan University, Wuxi, 214122, China.*

[c] School of Marine and Bioengineering, Yancheng Institute of Technology, Yancheng 224051, China.

‡ These authors contributed equally to this work.

* Corresponding author.

E-mail address: biowmc@126.com (M.C. Wu)

Contents:

1. Experimental section **4**

1.1 Materials 4

1.2 Mutagenesis 4

1.3 Mutant library screening assay 5

1.4 Preparation of *E. coli* cell suspension 6

1.5 Enzyme activity and enantioselectivity assays 6

1.6 Determination of regioselectivity coefficients 6

1.7 Computational simulation methods 7

1.8 Substrate scope analysis 7

1.9 Gram-scale preparation of (*R*)-**6b** at high concentration by *E.coli*/*Pveh1*^{Z6} 8

1.10 Semi-scale preparation of (*R*)-**1b**, **2b**, **3b**, **5b**, **8b** and **9b** by *E.coli*/*Pveh1*^{Z6} 8

2. Supporting section **9**

2.1 Tables S1-S5 ..... **9**

Table S1 Relative activity, product ee_p and conversion for single-site mutants towards *rac*-**6a**. 9

Table S2 The reported single EH-mediated enantioconvergent hydrolase of *rac*-epoxides. 10

Table S3 Substrate scope of *Pv*EH1 and mutants toward *rac*-**1a**–**9a**. 11

Table S4 List of primers for the mutagenesis of *Pv*EH1 12

Table S5 Chiral HPLC and GC chromatography methods of **1a**–**9a** and **1b**–**9b** 13

2.2 Figures S1-S23 ..... **14**

Fig. S1 Substrate-binding pocket of *Pv*EH1. 14

Fig. S2 Mutagenesis strategy of *Pv*EH1 with three continuous steps 15

Fig. S3 Primer design and random combinational mutagenesis of library 2 (a) or library 3 (b). 16

Fig. S4 Screening mutant library 3 towards *rac*-**6a** by chiral HPLC. 17

Fig. S5 SBP of WT (a) and *Pv*EH1^{Z6} (b). 18

Fig. S6 One hundred docking poses of WT or *Pv*EH1^{Z6} complex (*R*)- or (*S*)-**6a**. 19

Fig. S7 Non-binding interactions between WT (a and b) and *Pv*EH1^{Z6} (c and d) with (*R*)- and (*S*)-**6a** 20

Fig. S8. Compared with the 3-D structures of reported EHs. 21

Fig. S9 Enantioconvergence of WT and five mutants toward *rac*-**1a**–**3a** and **5a**–**9a** to access corresponding (*R*)-1,2-diols. 22

Fig. S10 Chiral GC spectra of *rac*-**6a** (a), (*R*)-**6a** (b) and (*S*)-**6a** (c). 23

Fig. S11 Chiral HPLC spectra for the hydrolysis of (*R*)-**6a** (a), (*S*)-**6a** (b) and *rac*-**6a** (c) catalysed by WT and mutants 24

Fig. S12 Chiral HPLC spectra for the hydrolysis of (*R*)-**1a** (a) and (*S*)-**1a** (b) catalysed by WT, *Pv*EH^{Z6} and *Pv*EH^{Z7}. 25

Fig. S13 Chiral HPLC spectra for the hydrolysis of (*R*)-**2a** (a) and (*S*)-**2a** (b) catalysed by WT, *Pv*EH^{Z6} and *Pv*EH^{Z7}. 26

Fig. S14 Chiral HPLC spectra for the hydrolysis of (*R*)-**5a** (a) and (*S*)-**5a** (b) catalysed by WT, *Pv*EH^{Z6} and *Pv*EH^{Z7}. 27

Fig. S15 Chiral HPLC spectra for the enantioconvergent hydrolysis of *rac*-**1a** (a) by WT (b), *Pv*EH^{Z6} (c) and *Pv*EH^{Z7} (d)..28

Fig. S16 Chiral HPLC spectra for the enantioconvergent hydrolysis of *rac*-**2a** (a) by WT (b), *Pv*EH^{Z6} (c) and *Pv*EH^{Z7} (d)..29

Fig. S17 Chiral HPLC spectra for the enantioconvergent hydrolysis of *rac*-**3a** (a) by WT (b), *Pv*EH^{Z6} (c) and *Pv*EH^{Z7} (d)..30

Fig. S18 Chiral HPLC spectra for the enantioconvergent hydrolysis of *rac*-**4a** (a) by WT (b), *Pv*EH^{Z6} (c) and *Pv*EH^{Z7} (d)..31

Fig. S19 Chiral HPLC spectra for the enantioconvergent hydrolysis of *rac*-**5a** (a) by WT (b), *Pv*EH^{Z6} (c) and *Pv*EH^{Z7} (d)..32

Fig. S20 Chiral HPLC spectra for the enantioconvergent hydrolysis of *rac*-**6a** (a) by WT (b), *Pv*EH^{Z6} (c) and *Pv*EH^{Z7} (d)..33

Fig. S21 Chiral HPLC spectra for the enantioconvergent hydrolysis of *rac*-**7a** (a) by WT (b), *Pv*EH^{Z6} (c) and *Pv*EH^{Z7} (d)..34

Fig. S22 Chiral HPLC spectra for the enantioconvergent hydrolysis of *rac*-**8a** (a) by WT (b), *Pv*EH^{Z6} (c) and *Pv*EH^{Z7} (d)..35

Fig. S23 Chiral GC spectra for the enantioconvergent hydrolysis of *rac*-**9a** (a) by WT (b), *Pv*EH^{Z6} (c) and *Pv*EH^{Z7} (d). 36

2.3 ^{1}H NMR spectra of *rac*-epoxides 37

2.4 ^{1}H NMR spectra of (*R*)-1,2-diols.....40

Reference 43

1. Experimental section

1.1 Materials

E. coli BL21(DE3) and pET-28a(+) (Novagen, Madison, WI) were used for the construction of recombinant plasmid and expression of *Pv*EH1 or mutants. Recombinant *E. coli/pveh1* and *E. coli/pveh1*^{Y3} harboring corresponding plasmid pET28a-*pveh1* and pET28a-*pveh1*^{Y3} were constructed and stored in our lab.[1] The PrimeSTAR HS DNA polymerase and *Dpn*I were purchased from TaKaRa (Dalian, China) for the construction of *Pv*EH1 mutants.

Racemic epoxides of styrene oxide (SO, **1a**) and *p*-bromostyrene oxide (*p*BrSO, **8a**) were purchased from Sigma-Aldrich. Racemic epoxides of *p*-nitrostyrene oxide (*p*NSO, **2a**), *m*-nitrostyrene oxide (*m*NSO, **3a**), *o*-nitrostyrene oxide (*o*NSO, **4a**), *p*-chlorostyrene oxide (*p*CSO, **5a**), *m*-chlorostyrene oxide (*m*CSO, **6a**), *p*-methylstyrene oxide (*p*MeSO, **7a**) and *p*-fluorostyrene oxide (*p*FSO, **9a**) were synthesized in our lab. Enantiopure epoxides of (*R*)-**1a, 2a**, **5a**, **6a** and (*S*)-**1a**, **2a**, **5a**, **6a** (> 99 ee_s) were prepared by the EH-mediated kinetic resolution of *rac*-**1a**, **2a**, **5a** and **6a** in our lab.

High-performance liquid chromatography (HPLC) was performed using a Waters e2695 apparatus (Waters, Milford, MA) equipped with a 2489 UV−vis detector. Gas chromatograph (GC) was performed using a GC-2014 apparatus (Shimadzu, Tokyo, Japan) equipped a flame ionization detector. ^{1}H NMR were performed on a Bruker 400 MHz spectrometer (Massachusetts, USA).

1.2 Mutagenesis

The mutagenesis of *Pv*EH1 was performed by PrimeSTAR HS DNA polymerase using a two-step whole-plasmid PCR method.[2] The primers were designed and synthesized as listed in **Table S4**. The 25 μL PCR reaction mixture typically contained 5 μL 5 × PrimeSTAR buffer (Mg^{2+}), 2 μL dNTP mixture, 0.5 μL template plasmid (50 ng/μL), 0.2 μL forward primer and 0.2 μL reverse primer (10 μM) for first-round PCR (PCR^{1st}) or 4 μL megaprimer for second-round PCR, 0.25 μL PrimeSTAR HS DNA polymerase (2.5 U/μL) and suitable volume of dd H_2O. PCR^{1st} conditions: a denaturation at 95 °C for 4 min, followed by 30 cycles of at 98 °C for 10 s, 55 °C for 5 s and 72 °C for 1000 bp/min, and an extra elongation at 72 °C for 10 min. PCR^{2nd} conditions: a denaturation at 95 °C for 4 min, followed by 25 cycles of at 98 °C for 10 s, 52 °C for 15 s and 72 °C for 1000 bp/min, and a final extension at 72 °C for 10 min. PCR^{1st} and PCR^{2nd} products were analyzed on agarose gel by electrophoresis. Each of PCR^{2nd} product was digested by 1 μL *Dpn* I, transformed into *E. coli* BL21(DE3) competent cells, and cultured in Luria–Bertani solid plate containing 50

μg/mL kanamycin.

Site-directed mutagenesis for library 1 Using pET28a-*pveh1* plasmid as a template, each of mutation primer (**Table S4**, library 1) as forward primer and pET28a-R as a universal reverse primer, PCR^{1st} was performed for the amplification of megaprimer. Subsequently, using pET28a-*pveh1* plasmid as a template and PCR^{1st} product as megaprimer, PCR^{2nd} was performed for the amplification of whole-plasmid conditions. All single-site mutants in mini-library 1 were validated by Sanger sequencing.

Random combinational mutagenesis for library 2 Five mutants V106I, M129L, M160A, M175I and S178T were divided into group 1. Random combinational mutagenesis was performed using pET28a-*pveh1* plasmid as a template (**Fig. S3a**) as reported method with slight modification.[3] Namely, PCR^{1st} was carried out using a mixed primers V106-F1, V106I-F1, M129-F1, M129-R1, M129L-F1, M160-F1, M160-R1, M160A-F1, M175/S178-R1, M175/S178-R1, M175/S178-R1, M175I-R1, S178T-R1 and M175I/S178T-R (**Table S4**, library 2) for the amplification of mixed megaprimers. Subsequently, using pET28a-*pveh1* plasmid as a template and PCR^{1st} product as mixed megaprimers, PCR^{2nd} was carried out for the amplification of mixed whole-plasmid conditions. One hundred *E. coli* transformants were picked up for activity screening by colorimetric assay.

Random combinational mutagenesis for library 3 Four mutants W102L, L105I, Y149L and P184W were included into group 2. Random combinational mutagenesis was performed using pET28a-*pveh1*^{Z4} plasmid as a template (**Fig. S3b**). Similarly, PCR^{1st} was performed using a mixed primers W102/L105-F2, W102L-F2, L105I-F2, W102L/L105I-F2, Y149-F2, Y149-R2, Y149L-F2, Y149L-R2, P184-R2 and P184W-R2 (**Table S4**, library 3) for the amplification of mixed megaprimers. Subsequently, using PCR^{1st} as mixed megaprimers, PCR^{2nd} was carried out for the amplification of mixed whole-plasmid conditions. Sixty *E. coli* transformants were picked up for enantioconvergence screening by chiral HPLC. *E. coli* transformants with both ee_p and c values > 70% were selected for DNA sequencing (**Fig. S4**)

1.3 Mutant library screening assay

E. coli transformants in library 2 and 3 were picked up and grown in 1.5 mL 96-well plate containing 1 ml of LB medium with 50 μg kanamycin. The plate was incubated at 37 °C for 2 h, and then the expression of recombinant EH was induced with 0.5 mM IPTG at 20 °C for 10 h. *E. coli* cell pellets was collected by centrifuging for 20 min at 3000 rpm.

Activity screening by colorimetric assay. *E. coli* cell pellets resuspended in 475 μL phosphate buffer (100 mM, pH 7.0) was mixed with 25 μL *rac*-**6a** (200 mM in methanol). After incubation at 25 °C for 2 h, reaction was stopped by adding 50 μL 50 mM 4-(*p*-nitrobenzyl)pyridine (NBP). The plate was incubated at 80 °C for 30 min, cooled by an ice-bath, and added 500 μL 50% triethylamine (v/v) as developer. The absorbance, inversely proportional to the EH activity, was measured at 560 nm.

Enantioconvergence screening by chiral HPLC. *E. coli* cell pellets resuspended in 490 μL xphosphate buffer (100 mM, pH 7.0) was mixed with 50 μL *rac*-**6a** (200 mM in methanol). After incubation at 25 °C for 12 h, the reaction solution was extracted with 1 mL ethyl acetate and assayed by chiral HPLC to determine the conversion of *rac*-**6a** and ee_p of (*R*)-**6b** (**Table S5**). The *c* was calculated using the equation: $c = (A_p \times \varepsilon) / (A_p \times \varepsilon + A_s)$,[4] where A_p and A_s are the peak areas of product diol and retained epoxide, while ε is the corresponding molar attenuation coefficient. $ee_p = [(R_p - S_p) / (R_p + S_p)] \times 100\%$, where R_p and S_p are the concentrations of (*R*)- and (*S*)-diol.

1.4 Preparation of *E. coli* cell suspension

E. coli transformants of *Pv*EH1 and its mutants were separately incubated in LB medium (containing 50 μg/mL kanamycin) at 37°C overnight. Then, 2% (v/v) culture was inoculated into the fresh 100 LB medium and cultured at 37 °C until OD_{600} reached 0.6–0.8. The expression of *Pv*EH1 and mutants were induced by 0.5 mM IPTG and incubated at 20 °C for 10 h. *E. coli* cells were harvested and resuspended in phosphate buffer (100 mM, pH 7.0) to a final concentration of 100 or 200 mg wet cells/mL.

1.5 Enzyme activity and enantioselectivity assays

The EH activity towards *rac*-**6a** was measured as follows: 100 μL cell suspension (100 mg wet cells/mL) mixed with 375 μL 100 mM phosphate buffer (pH 7.0) was preincubated at 25 °C for 5 min. Then, reaction was started by addition of 25 μL *rac*-**6a** (200 mM). After incubation at 25 °C for 10 min, aliquots of 100 μL reaction solution were withdrawn, extracted with 1 mL ethyl acetate, assayed by chiral HPLC to determine the *c* of *rac*-**6a** (**Table S5**), and chiral GC to determine ee_s of (*R*)-**6a** (**Fig. S10**). One EH activity unit (U) was defined as the amount of *E. coli* wet cells producing 1 μmol **6b** per minute under the given assay conditions. The enantioselectivity towards *rac*-**6a**, quantitatively described by its enantiomeric ratio (*E* value), was calculated according the equation $E = \ln [(1 - c) \times (1 - ee_s)] / \ln [(1 - c) \times (1 + ee_s)]$.[5]

1.6 Determination of regioselectivity coefficients

Regioselectivity coefficients α_S and β_R were applied to quantitatively evaluate the preference attacking on

benzylic carbon C_α of (*S*)-enantiomer and on terminal carbon C_β of (*R*)-enantiomer, respectively.[6] The regioselectivity coefficients of *Pv*EH1 and its mutants was determined as follows: 475 μL cell suspension (100 mg wet cells/mL) mixed with 25 μL (*S*)- or (*R*)-**1a**, **2a**, **5a** or **6a** (100 mM). After incubation at 25 °C for 12 h, the reaction solution was extracted with 1 mL ethyl acetate, and assayed by chiral HPLC (**Table S5**). The regioselectivity coefficient, α_S or β_R, was directly calculated based on concentration ratio of its corresponding produced (*R*)- and (*S*)-diol.

1.7 Computational simulation methods

Homology modeling of 3-D structure Using the known crystal structure of a *Vigna radiata* EH1 (*Vr*EH1, PDB: 5XMD) as the template, the 3-D structures of *Pv*EH1 and its mutants were modelled using the SWISS-MODEL (https://swissmodel.expasy.org/).[7] The substrate-binding pocket (SBP) of protein structures was visualized by PyMOL software (http://pymol.org/).

Molecular docking simulation The 3-D structures of (*R*)- and (*R*)-**6a** were handled and minimized by applying CHARMm force field using Discovery Studio 2018. The homology modelled WT and *Pv*EH1^{Z6} were used as the receptor proteins for docking ligand (*R*)- or (*R*)-**6a** by AutoDock 4.2 program.[8] The grid box was set for the size of 44 × 40 × 50 with the spacing of 0.375 Å. The center grid box was defined by the coordinate of OD1 of D101. The molecule docking simulation was performed with flexible ligand by genetic algorithm to locate the suitable binding orientation. One hundred docking poses were collected for analysis the preferred binding modes.

Molecular dynamics simulations Molecular docking configurations of WT-(*R*)-**6a**, WT-(*S*)-**6a**, *Pv*EH1^{Z6}-(*R*)-**6a**, and *Pv*EH1^{Z6}-(*S*)-**6a** with the lowest binding energy were subjected to 5 ns molecular dynamics (MD) simulations using Discovery Studio 2018. Firstly, the molecule-docked complex structure was treated with CHARMm force field and encapsulated by a cubic solvent under explicit periodic boundary conditions. Then, two stage of energy minimization were conducted by 1000 step steepest descent and 2000 step conjugate gradient algorithms. Secondly, the harmonic restraints were created at O-atom of epoxide ring and hydroxyl H-atoms of Y150 and Y243 with a force constant of 10 kcal/(mol·Å^2). The energy minimized system was heated from 50 to 300 K, and a 100 ps equilibration process was performed at 300 K. Finally, a 5 ns MD simulation was performed under at NPT condition at 300 K with the hydrogen bond fixed using the SHAKE algorithm.[9] Distances (d_α and d_β) between nucleophilic OD1 of D101 and C_α and C_β of epoxide ring was monitored according to trajectory analysis during MD simulations.

1.8 Substrate scope analysis

Aliquots of 485 μL *E. coli* cell suspension (100 mg wet cells/mL) mixed with 5% Tween-20 (v/v) and 10 mM *rac*-**1a**−**9a** were incubated at 25 °C for 12 h, respectively. Then, reaction solution was extracted with 1 mL ethyl acetate, and assayed by chiral HPLC to determine the *c* of *rac*-**1a**−**9a** and the ee_p of (*R*)-**1b**−**9b** (**Table S4**).

1.9 Gram-scale preparation of (*R*)-6b at high concentration by *E.coli*/*Pveh1*^{Z6}

The enantioconvergent hydrolysis of *rac*-**6a** were performed in 50 mL phosphate buffer (100 mM, pH 7.0) containing 10 g *E.coli*/*Pveh1*^{Z6} wet cells (about 1.6 g dry cells), 10% Tween-20 (v/v) and 2.7 g *rac*-**6a** (350 mM 53.9 g/L) at 25 °C and 220 rpm. During the hydrolytic course, aliquots of 20 μL sample solution were periodically drawn out, extracted with 1 mL ethyl acetate, and analyzed by chiral HPLC to monitor the conversion of *rac*-**6a** and the ee_p of (*R*)-**6b**. When conversion reached over 99%, the total reaction solution was extracted with 20 mL petroleum ether twice to remove the unreacted **6a**. Then, the aqueous phase was extracted with 20 mL ethyl acetate thrice. The pooled ethyl acetate fractions were washed by saturated NaCl thrice, dried over anhydrous sodium sulphate, and purified by silica gel column chromatography, followed by concentrating under reduced pressure.

1.10 Semi-scale preparation of (*R*)-1b, 2b, 3b, 5b, 8b and 9b by *E.coli*/*Pveh1*^{Z6}

The enantioconvergent hydrolysis of *rac*-**1a**, **2a**, **3a**, **5a**, **8a** and **9a** was individually performed in 10 mL phosphate buffer (100 mM, pH 7.0) containing 2 g *E.coli*/*Pveh1*^{Z6} wet cells, 10% methanol (v/v) and 50 or 100 mM *rac*-epoxide at 25 °C and 220 rpm for 8 h (**Table 2**). Then, 20 μL sample solution was drawn out, extracted with 1 mL ethyl acetate, and analyzed by chiral HPLC to determine the *c* of *rac*-epoxide and the ee_p of (*R*)-1,2-diol (Table 2). Total reaction solution was extracted with 10 mL petroleum ether twice to remove the unreacted epoxide. Then, aqueous phase was extracted with 10 mL ethyl acetate thrice. The pooled ethyl acetate fractions were washed by saturated NaCl thrice, dried over anhydrous sodium sulphate, followed by concentrating under reduced pressure.

2. Supporting section

2.1 Tables S1-S5

Table S1 Relative activity, product ee_p and conversion for single-site mutants towards *rac*-6a.

Step	Code	Mutant	Relative activity (%)	ee_p (%)	c (%)
	WT	none	100	1.0 (*R*)	99.9
Step 1	*Pv*EH1$^{Z1\text{-}1}$	W102L	47.0	80.6 (*R*)	87.1
	*Pv*EH1$^{Z1\text{-}2}$	W102I	43.1	75.6 (*R*)	81.5
	*Pv*EH1$^{Z1\text{-}3}$	W102T	32.8	6.5 (*R*)	99.2
	*Pv*EH1$^{Z1\text{-}4}$	L105I	138	73.7 (*R*)	99.8
	*Pv*EH1$^{Z1\text{-}5}$	V106L	14.8	3.2 (*R*)	94.0
	*Pv*EH1$^{Z1\text{-}6}$	V106I	138	-13.5 (*R*)	97.5
	*Pv*EH1$^{Z1\text{-}7}$	V106W	10.1	23.4 (*R*)	21.4
	*Pv*EH1$^{Z1\text{-}8}$	V106T	13.8	-2.31 (*R*)	93.3
	*Pv*EH1$^{Z1\text{-}9}$	M129L	165	-9.5 (*R*)	99.7
	*Pv*EH1$^{Z1\text{-}10}$	Y149L	21.1	55.1 (*R*)	94.1
	*Pv*EH1$^{Z1\text{-}11}$	Y149I	6.3	26.5 (*R*)	6.4
	*Pv*EH1$^{Z1\text{-}12}$	Y149W	ND	ND	ND
	*Pv*EH1$^{Z1\text{-}13}$	Y149T	ND	ND	ND
	*Pv*EH1$^{Z1\text{-}14}$	M160A	150	3.3 (*R*)	99.6
	*Pv*EH1$^{Z1\text{-}15}$	M175I	125	6.3 (*R*)	99.9
	*Pv*EH1$^{Z1\text{-}16}$	S178L	81.5	4.1 (*R*)	99.1
	*Pv*EH1$^{Z1\text{-}17}$	S178I	71.5	4.1 (*R*)	98.4
	*Pv*EH1$^{Z1\text{-}18}$	S178W	26.2	-3.3 (*R*)	92.5
	*Pv*EH1$^{Z1\text{-}19}$	S178T	136	-15.0 (*R*)	99.2
	*Pv*EH1$^{Z1\text{-}20}$	P184L	105	27.3 (*R*)	99.5
	*Pv*EH1$^{Z1\text{-}21}$	P184I	31.0	15.8 (*R*)	99.4
	*Pv*EH1$^{Z1\text{-}23}$	P184W	72.4	58.2 (*R*)	99.3
	*Pv*EH1$^{Z1\text{-}24}$	P184T	20.1	7.36 (*R*)	99.6
Step 2	*Pv*EH1^{Z1}	V106I/M160A	122	6.8 (*R*)	94.1
	*Pv*EH1^{Z2}	V106I/M160A/M175I	111	-3.5 (*R*)	93.6
	*Pv*EH1^{Z3}	V106I/M160A/S178T	296	-1.6 (*R*)	99.4
	*Pv*EH1^{Z4}	V106I/M160A/M175I/S178T	315	9.0 (*R*)	99.9
	*Pv*EH1^{Z5}	V106I/M129L/M160A/M175I/S178T	171	2.9 (*R*)	99.0
Step 3	*Pv*EH1^{Z6}	L105I/V106I/M160A/M175I/S178T/P184W	362	96.2 (*R*)	99.2
	*Pv*EH1^{Z7}	L105I/V106I/Y149L/M160A/M175I/S178T/P184W	151	95.3 (*R*)	98.9
	*Pv*EH1^{Z8}	W102L/L105I/V106I/Y149L/M160A/M175I/S178T/P184W	34.3	98.3 (*R*)	69.7

[a] Mutant residues V106I, M129L, M160A, M175I and S178T in group 1 are shown in blue, while residues W102L, L105I, Y149L and P184W in group 2 are shown in red.

Table S2 The reported single EH-mediated enantioconvergent hydrolase of *rac*-epoxides.

Substrate	EH	Concentration (mM)	*c* (%)	ee_p (%)	α_S (%)	β_R (%)	Reference
1a	*Cc*EH	10	93	90 (*R*)			10
	*St*EH1	4	100	86 (*R*)	98	93	11
	Kua2	3.5	100	77 (*R*)			12
	Kua8	3.5	100	71 (*R*)			12
	*Vr*HE2^{M263N}	1	>99	92 (*R*)			13
	*Vr*EH3	100	>99	92.5 (*R*)	97.2	98.2	14
	*An*EH$_{M200}$	4	100	70.1 (*R*)	93	78	15
	SgcF^{Q237M}	2	100	89.8 (*R*) [a]	97.9	87.7	16
	*Pv*EH1^{Z6}	10	99.1	89.5 (*R*)	98.2	91.9	This study
	*Pv*EH1^{Z7}	10	99.2	92.1 (*R*)	99.6	92.2	This study
2a	*Cc*EH	10	80	NI (*R*)			10
	Kua2	3.5	100	87 (*R*)			12
	Kua8	3.5	100	22 (*R*)			12
	*Vr*EH1	2	> 99	70 (*R*)	83	87	17
	*Vr*HE2^{M263N}	100	> 99	98 (*R*)	99	99	13
	*Vr*EH3	10	> 99	85.2 (*R*)			14
	*Pv*EH1^{Z6}	10	98.1	89.6 (*R*)	92.3	95.5	This study
	*Pv*EH1^{Z7}	10	97.5	98.3 (*R*)	99.7	98.5	This study
3a	*Cc*EH	10	NA [b]				10
	*Vr*HE2^{M263N}	1	> 99	80 (*R*)			13
	*Vr*EH3	10	> 99	60.9 (*R*)			14
	*Pv*EH1^{Z6}	10	99.3	95.4 (*R*)			This study
	*Pv*EH1^{Z7}	10	99.6	97.3 (*R*)			This study
5a	*Cc*EH	110	NI [c]	95 (*R*)	94	99	10
	*St*EH1	4	100	74 (*R*)	97	92	11
	Kua2	3.5	100	85 (*R*)	95	90	12
	Kua2 variant F:13-B11	6.6	100	93 (*R*)	96	97	18
	Kua8	3.5	100	13 (*R*)	34	80	12
	*Vr*EH3	20	>99	88.2 (*R*)			14
	*An*EH$_{M200}$ variant H:12-A1	4	100	70.5 (*R*)	87	83	15
	*Pv*EH1^{Z6}	10	99.9	83.9 (*R*)	98.3	85.4	This study
	*Pv*EH1^{Z7}	10	98.7	90.0 (*R*)	98.9	91.1	This study
6a	*Cc*EH	10	36	NI (*R*)			10
	*St*EH1	4	100	91 (*R*)	97	94	11
	Kua2	3.5	100	91 (*R*)	99	92	12
	Kua8	3.5	100	45 (*R*)	96	48	12
	*Vr*EH3	20	99	50.3 (*R*)			14
	*Pv*EH1^{Z6}	350	99.2	96.8 (*R*)	98.5	97.7	This study
	*Pv*EH1^{Z7}	10	98.1	95.7 (*R*)	99.2	96.2	This study
7a	*Cc*EH	10	NA				10
	*Pv*EH1^{Z6}	10	99.2	68.8 (*R*)			This study
8a	*Pv*EH1^{Z6}	10	98.8	82.6 (*R*)			This study
	*Pv*EH1^{Z7}	10	98.4	94.9 (*R*)			This study
9a	*Pv*EH1^{Z6}	10	100	89.5 (*R*)			This study
	*Pv*EH1^{Z7}	10	96.4	90.5 (*R*)			This study

[a] The ee_p was calculated according to the regioselectivity coefficients (α_S and β_R).

[b] NA represents no activity.

[c] NI represents no information.

Table S3 Substrate scope of *Pv*EH1 and mutants toward *rac*-1a−9a.

Substrate		*Pv*EH1		*Pv*EH1^{L105I}		*Pv*EH1^{P184W}		*Pv*EH1^{Y3}		*Pv*EH1^{Z6}		*Pv*EH1^{Z7}	
		c (%)	ee_p (%)	*c* (%)	ee_p (%)	*c* (%)	ee_p (%)	*c* (%)	ee_p (%)	*c* (%)	ee_p (%)	*c* (%)	ee_p (%)
1a	SO	99.1	33.6	99.2	70.4	99.5	55.1	99.1	87.9	99.1	89.5	98.2	92.0
2a	*p*NSO	99.3	50.3	97.8	58.6	98.9	79.9	99.5	64.7	98.1	89.6	98.5	98.3
3a	*m*NSO	99.7	14.7	99.9	44.9	99.4	63.2	99.4	52.3	99.3	95.4	99.6	97.3
4a	*o*NSO	11.4	1.0	19.5	-47.3	15.3	16.3	23.9	-27.9	76.7	7.2	35.4	47.0
5a	*p*CSO	98.2	51.4	98.8	64.4	99.3	62.3	99.4	73.0	99.9	83.9	98.7	90.1
6a	*m*CSO	99.9	1.0	99.8	73.7	99.3	58.1	99.3	69.7	99.2	96.8	98.1	95.7
7a	*p*MeSO	99.7	25.7	98.7	47.2	97.0	44.9	99.1	59.9	99.2	68.8	98.7	68.2
8a	*p*BrSO	99.2	37.1	96.6	58.0	99.5	62.8	96.5	68.2	98.8	82.6	98.4	94.9
9a	*p*FSO	98.7	13.6	100	72.5	98.2	53.3	100	63.5	100	89.5	98.7	90.5

[a.] The ee_p is the enantiomeric excess of (*R*)-diol. The reactions were performed with 10 mM *rac*-**1a-9a** using 100 mg/mL *E. coli* wet cells in a phosphate buffer (100 mM, pH 7.0) at 25 °C for 12 h.

Table S4 List of primers for the mutagenesis of *Pv*EH1

Library	Name	Sequence (5' to 3')[a]
Library 1	W102L-F	CTCGTTGCCCATGATCTCGGAGCCCTAGTAGGA
	W102I-F	CTCGTTGCCCATGATATTGGAGCCCTAGTAGGA
	W102T-F	CTCGTTGCCCATGATACCGGAGCCCTAGTAGGA
	L105I-F	CCATGATTGGGGAGCCATTGTAGGATGGTACACA
	V106L-F	GATTGGGGAGCCCTATTAGGATGGTACACATGT
	V106I-F	GATTGGGGAGCCCTAATAGGATGGTACACATGT
	V106W-F	GATTGGGGAGCCCTATGGGGATGGTACACATGT
	V106T-F	GATTGGGGAGCCCTAACAGGATGGTACACATGT
	M129L-F	CTCAGCGTCCCTTTCCTGCCCAGAAACCCA
	Y149L-F	CTTTATGGGGATGACTTATACATCTGCAGATTC
	Y149I-F	CTTTATGGGGATGACATCTACATCTGCAGATTC
	Y149W-F	CTTTATGGGGATGACTGGTACATCTGCAGATTC
	Y149T-F	CTTTATGGGGATGACACCTACATCTGCAGATTC
	M160A-F	AGGAACCAGGCAAGGCGGAAACTCTGTATGAC
	M175I-F	GAAGCAATCAAGAACATTCTGACAAGTAGGAGACC
	S178L-F	AAGAACATGCTTACACTGAGGAGACCAGGACCA
	S178I-F	AAGAACATGCTTACAATTAGGAGACCAGGACCA
	S178W-F	AAGAACATGCTTACATGGAGGAGACCAGGACCA
	S178T-F	AAGAACATGCTTACAACTAGGAGACCAGGACCA
	P184L-F	AGGAGACCAGGACCACTGATCCTCCCCAAAGAA
	P184I-F	AGGAGACCAGGACCAATTATCCTCCCCAAAGAA
	P184W-F	AGGAGACCAGGACCATGGATCCTCCCCAAAGAA
	P184T-F	AGGAGACCAGGACCAACAATCCTCCCCAAAGAA
	pET28a-R	GCCTTACTGGTTAGCAGAATG
Library 2	V106-F1	GATTGGGGAGCCCTAGTAGGATGGTACACATGT
	V106I-F1	GATTGGGGAGCCCTAATAGGATGGTACACATGT
	M129-F1	CTCAGCGTCCCTTTCATGCCCAGAAACCCA
	M129-R1	TGGGTTTCTGGGCATGAAAGGGACGCTGAG
	M129L-F1	CTCAGCGTCCCTTTCCTGCCCAGAAACCCA
	M129L-R1	TGGGTTTCTGGGCAGGAAAGGGACGCTGAG
	M160-F1	AGGAACCAGGCAAGATGGAAACTCTGTATGAC
	M160-R1	GTCATACAGAGTTTCCATCTTGCCTGGTTCCT
	M160A-F1	AGGAACCAGGCAAGGCGGAAACTCTGTATGAC
	M160A-R1	GTCATACAGAGTTTCCGCCTTGCCTGGTTCCT
	M175/S178-R1	TGGTCCTGGTCTCCTACTTGTAAGCATGTTCTTGATTGCTTC
	M175I-R1	TGGTCCTGGTCTCCTACTTGTAAGAATGTTCTTGATTGCTTC
	S178T-R1	TGGTCCTGGTCTCCTAGTTGTAAGCATGTTCTTGATTGCTTC
	M175I/S178T-R	TGGTCCTGGTCTCCTAGTTGTAAGAATGTTCTTGATTGCTTC
Library 3	W102/L105-F2	CTCGTTGCCCATGATTGGGGAGCCCTAATAGGATGGTACACA
	W102L-F2	CTCGTTGCCCATGATCTCGGAGCCCTAATAGGATGGTACACA
	L105I-F2	CTCGTTGCCCATGATTGGGGAGCCATTATAGGATGGTACACA
	W102L/L105I-F2	CTCGTTGCCCATGATCTCGGAGCCATTATAGGATGGTACACA
	Y149-F2	CTTTATGGGGATGACTACTACATCTGCAGATTC
	Y149-R2	GAATCTGCAGATGTAGTAGTCATCCCCATAAAG
	Y149L-F2	CTTTATGGGGATGACTTATACATCTGCAGATTC
	Y149L-R2	GAATCTGCAGATGTAAATGTCATCCCCATAAAG
	P184-R2	TTCTTTGGGGAGGATTGGTGGTCCTGGTCTCCT
	P184W-R2	TTCTTTGGGGAGGATCCATGGTCCTGGTCTCCT

[a] Mutation site codon is underlined. Mutation site codons of V106I, M129L, M160A, M175I and S178T in group 1 are shown in blue, while codons of W102L, L105I, Y149L and P184W in group 2 are shown in red.

Table S5 Chiral HPLC and GC chromatography methods of 1a–9a and 1b–9b

Compound	Column[a]	HPLC and GC condition[a]	Retention time for epoxide (min)	Retention time for diol (min)	ε[c]
1a, **1b**	OD-H	80:20, 220 nm, 0.8 mL/min	5.43 (*S*)/ 5.76 (*R*)	6.51 (*R*) / 6.90 (*S*)	6.1462
2a, **2b**	OD-H	80:20, 254 nm, 0.8 mL/min	8.40 (*R*)/(*S*)	9.74 (*R*) / 11.48 (*S*)	1.1827
3a, **3b**	OD-H	90:10, 254 nm, 0.8 mL/min	9.78 (*R*)/(*S*)	15.77 (*R*) / 18.30 (*S*)	1.1647
4a, **4b**	OD-H	90:10, 254 nm, 0.8 mL/min	7.16 (*R*) / 7.42 (*S*)	13.43 (*R*) / 16.85 (*S*)	1.3215
5a, **5b**	AS-H	90:10, 220 nm, 0.8 mL/min	6.815 (*R*)/ 7.95 (*S*)	13.91 (*S*)/ 16.01 (R)	1.0399
6a, **6b**	OD-H	90:10, 220 nm, 0.8 mL/min	5.797 (*S*)/(*R*)	9.61 (*R*)/ 10.861 (*S*)	1.2874
7a, **7b**	AS-H	90:10, 220 nm, 0.8 mL/min	6.08 (*R*)/ 6.73 (*S*)	12.22 (*S*)/ 14.44 (*R*)	1.2163
8a, **8b**	AS-H	90:10, 220 nm, 0.8 mL/min	7.40 (*R*)/ 8.75 (*S*)	14.96 (*S*)/ 17.67 (*R*)	1.1821
9a, **9b**	Cyclosil-B[b]	100 °C, 3 °C/min, to 130 °C, 10 °C/min, to 160 °C[b]	8.25 (*R*)/ 8.46 (*S*)	21.47 (*S*)/ 21.72 (*R*)	1.3601

[a] HPLC was performed using a Waters e2695 apparatus (Waters, Milford, MA) equipped with a Chiralpak ® AS-H or Chiralcel ® OD-H column (5 μm, 4.6 mm × 250 mm, Daicel, Japan) at the column temperature of 30 ºC. The mobile phase of *n*-hexane/isopropanol (90:10 or 80:20) was used at a flow rate of 0.8 mL/min, and monitored at 254 or 220 nm with a Waters 2489 UV-Vis detector.

[b] GC was performed with a GC-2010 apparatus (Shimadzu, Tokyo, Japan) equipped with a chiral Cyclosil-B (30 m × 0.25 mm × 0.25 μm; Agilent, Santa Clara, CA) and a flame ionization detector. The injector and detector were 250 °C, carrier gas was N_2 at a flow rate of 3 mL/min, injection volume was 1 μL, and the split ratio was 50:1.

[c] ε is the extinction coefficient of epoxide/diol. Conversion ratio (c) = $(A_{diol} \times \varepsilon)/(A_{diol} \times \varepsilon + A_{epoxide})$. $A_{epoxide}$ and A_{diol} represent the peak area of epoxides or their corresponding vicinal diols.

2.2 Figures S1-S23

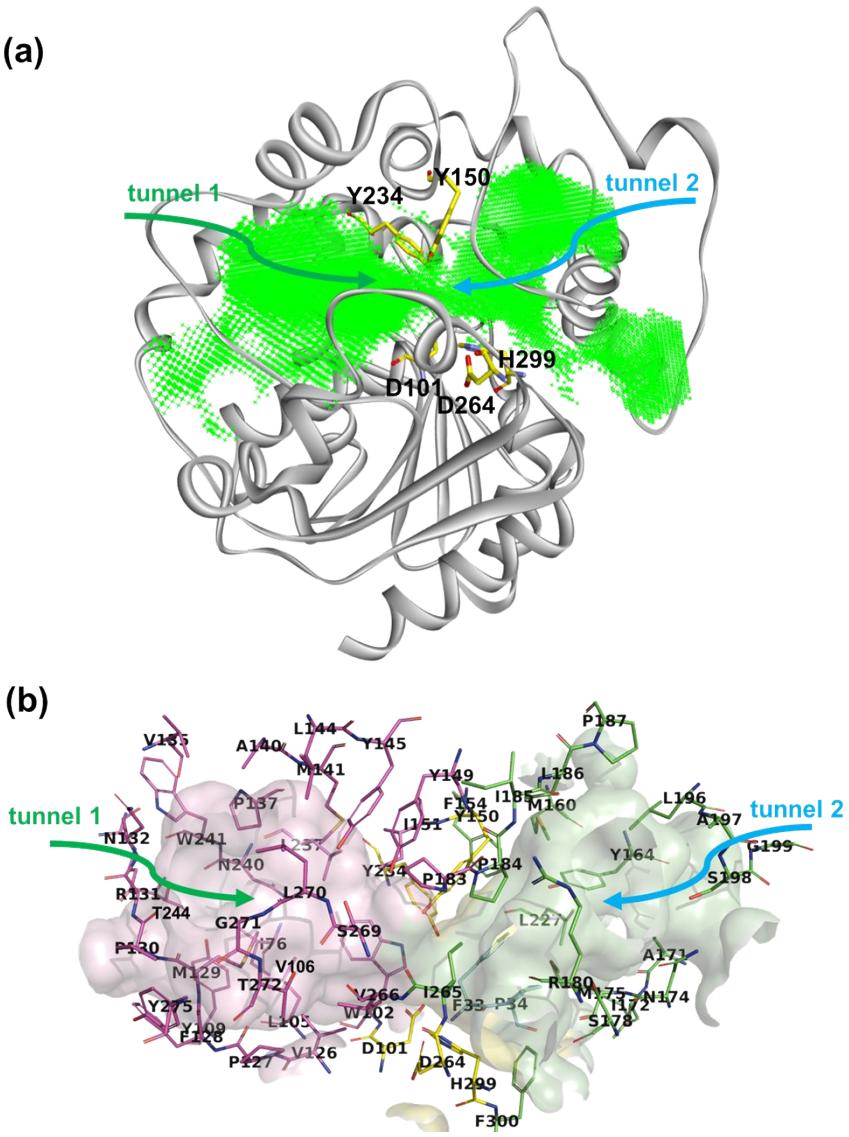

Fig. S1 Substrate-binding pocket of *Pv*EH1. (a) Substrate-binding pocket of *Pv*EH1 were generated in Discovery studio 2018. **(b)** Substrate-binding pocket of *Pv*EH1 were generated in PyMol (www.pymol.org). Active site including the catalytic triad D101-H299-D264 and two tyrosine Y150 and Y234 are shown in yellow sticks. The substrate tunnel 1 and tunnel are shown in pink and green surface, respectively. The substrate tunnel 1 is composed of 32 residues I76, W102, V106, L105, Y109, V126, P127, F128, M129, P130, R131, N132, V135, P137, A140, M141, L144, Y145, Y149, I151, P183, L234, L237, N240, W241, T244, V266, S269, L270, G271, T272 and Y275. The substrate tunnel 2 is composed of 22 residues F33, P34, F154, M160, Y164, A171, I172, N174, M175, S178, R180, P184, I185, L186, P187, L196, A197, S198, G199, L277, I265 and F300.

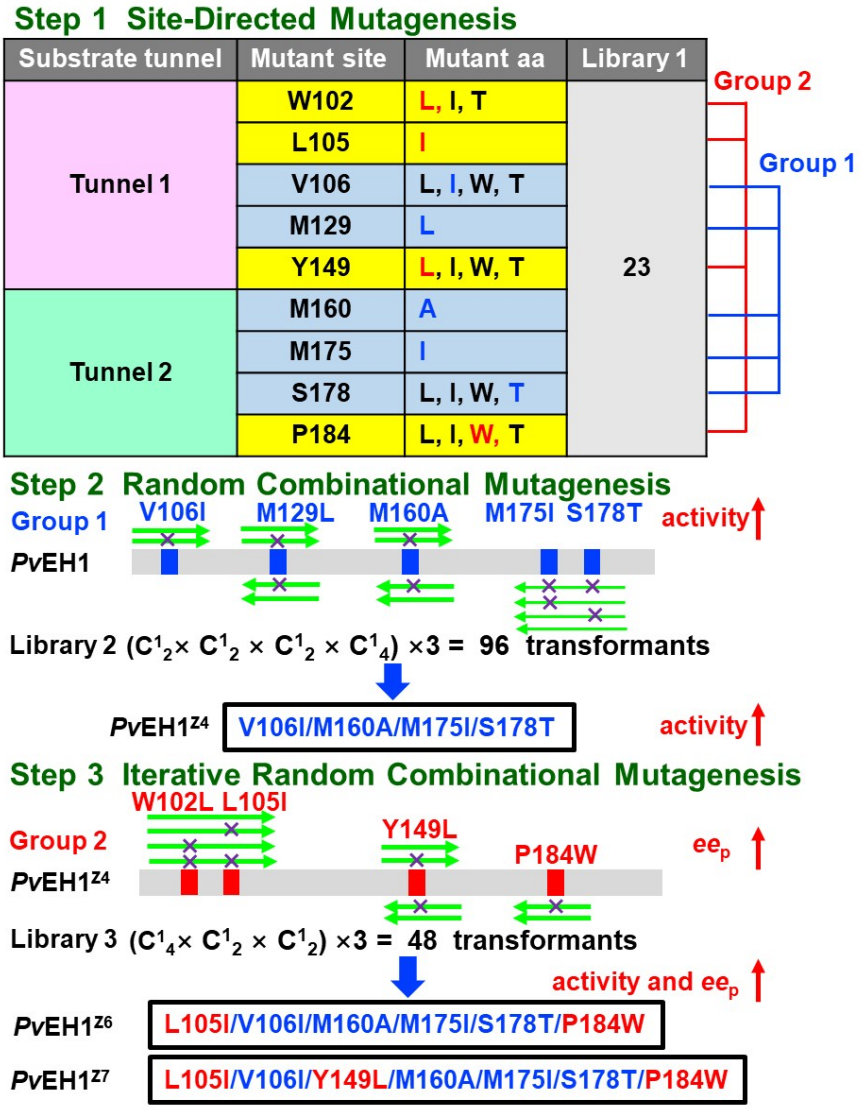

Fig. S2 Mutagenesis strategy of *Pv*EH1 with three continuous steps

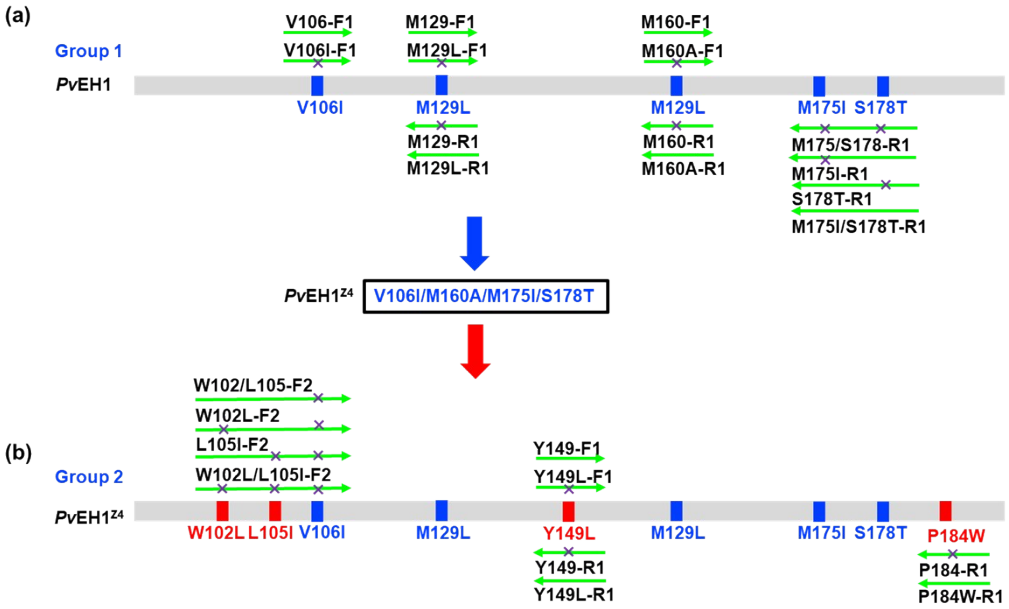

Fig. S3 Primer design and random combinational mutagenesis of library 2 (a) or library 3 (b).

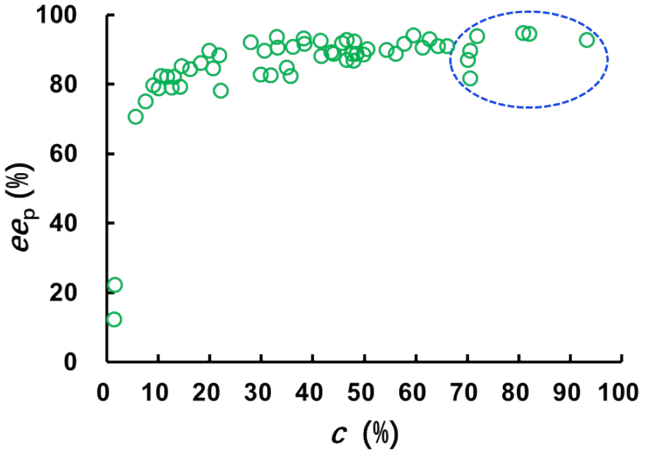

Fig. S4 Screening mutant library 3 towards *rac*-6a by chiral HPLC. Scatter diagram was plotted using ee_p of (*R*)-**6b** and conversion as ordinate and abscissa, respectively.

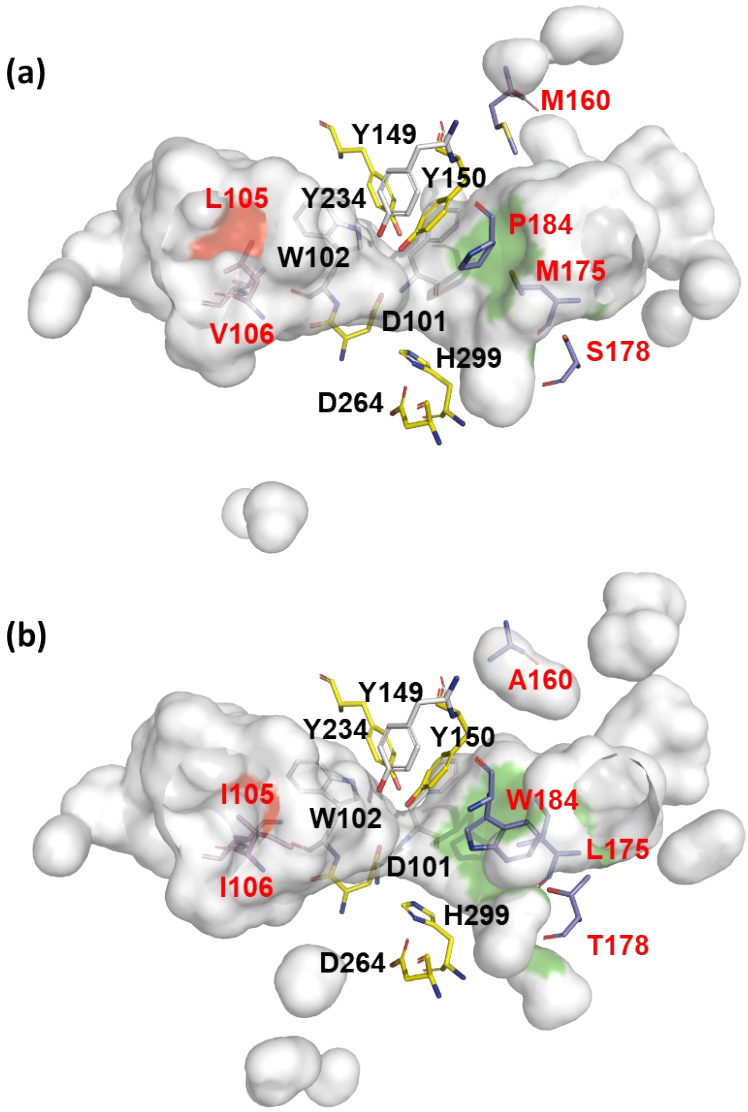

Fig. S5 SBP of WT (a) and ***Pv*EH1^{Z6} (b).** The catalytic triad D101-H299-D264, two tyrosines Y150 and Y234 are shown in yellow stick. The mutant residues L/I105 and V/I106 in tunnel 1 are shown in pink stick and red surface. The mutant residues M/A160, M/L175, S/T178 and P/W184 in tunnel 2 are shown in blue stick and green surface.

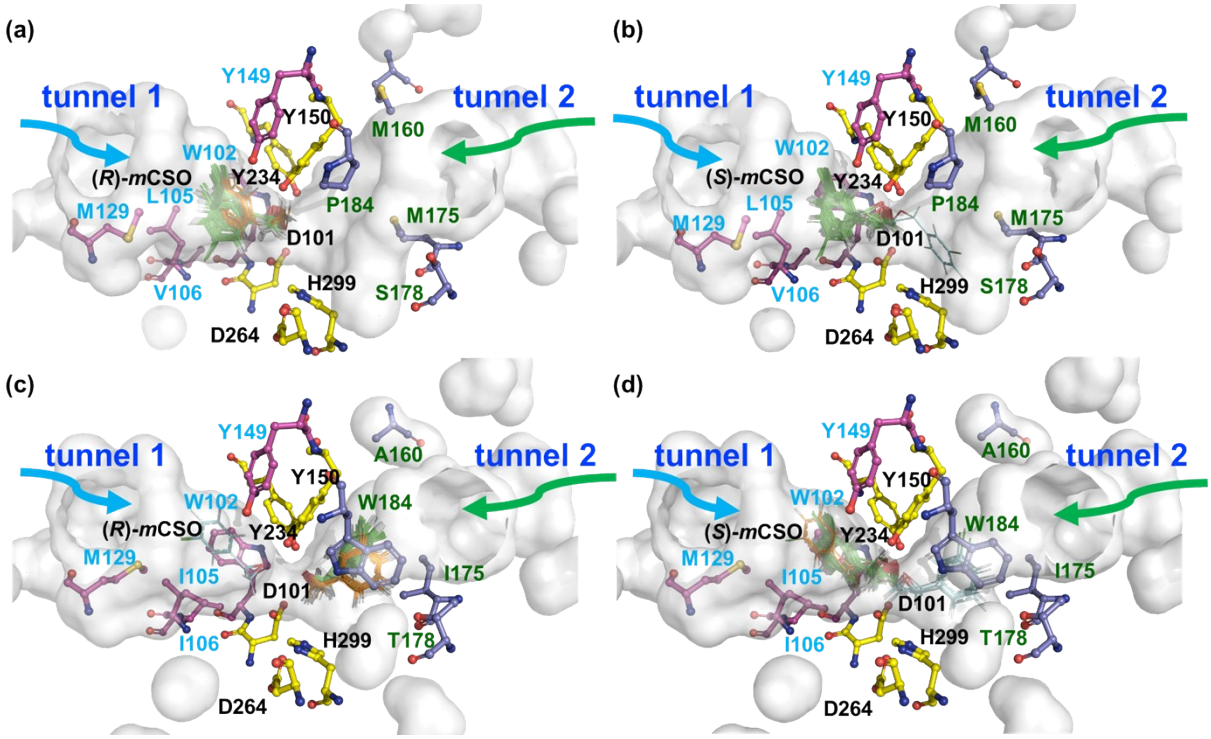

Fig. S6 One hundred docking poses of WT or *Pv*EH1^{Z6} complex (*R*)- or (*S*)-6a. (**a**) Molecule docking poses of WT with (*R*)-**6a**. (**b**) Molecule docking poses of WT with (*S*)-**6a**. (**c**) Molecule docking poses of *Pv*EH1^{Z6} with (*R*)-**6a**. (**d**). Molecule docking poses of *Pv*EH1^{Z6} with (*S*)-**6a**.

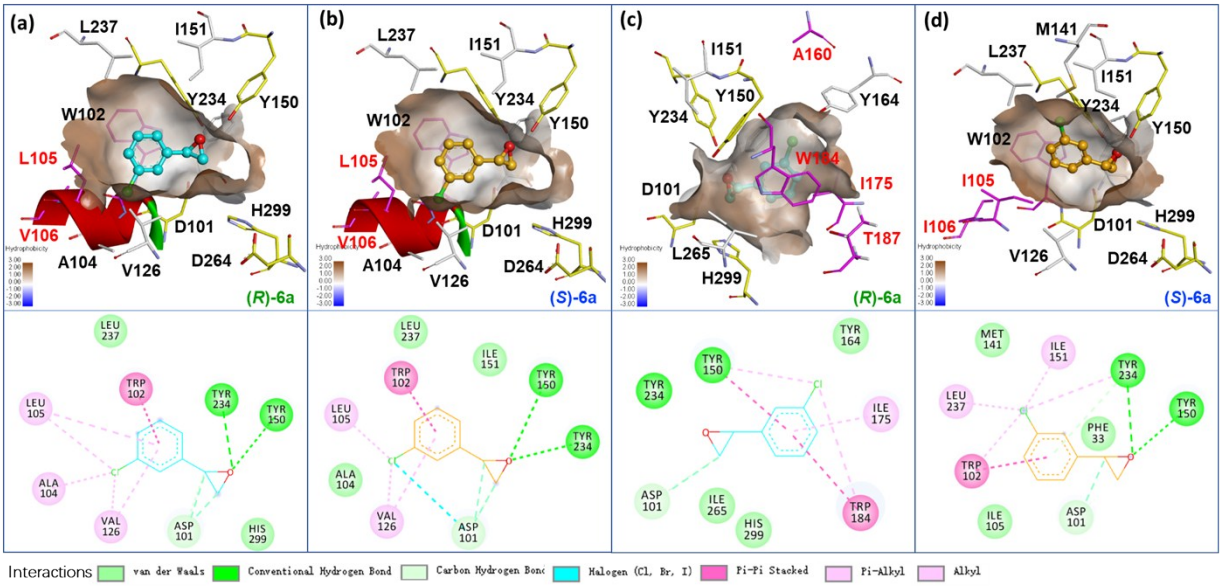

Fig. S7 Non-binding interactions between WT (a and b) and *Pv*EH1^{Z6} (c and d) with (*R*)- and (*S*)-6a.

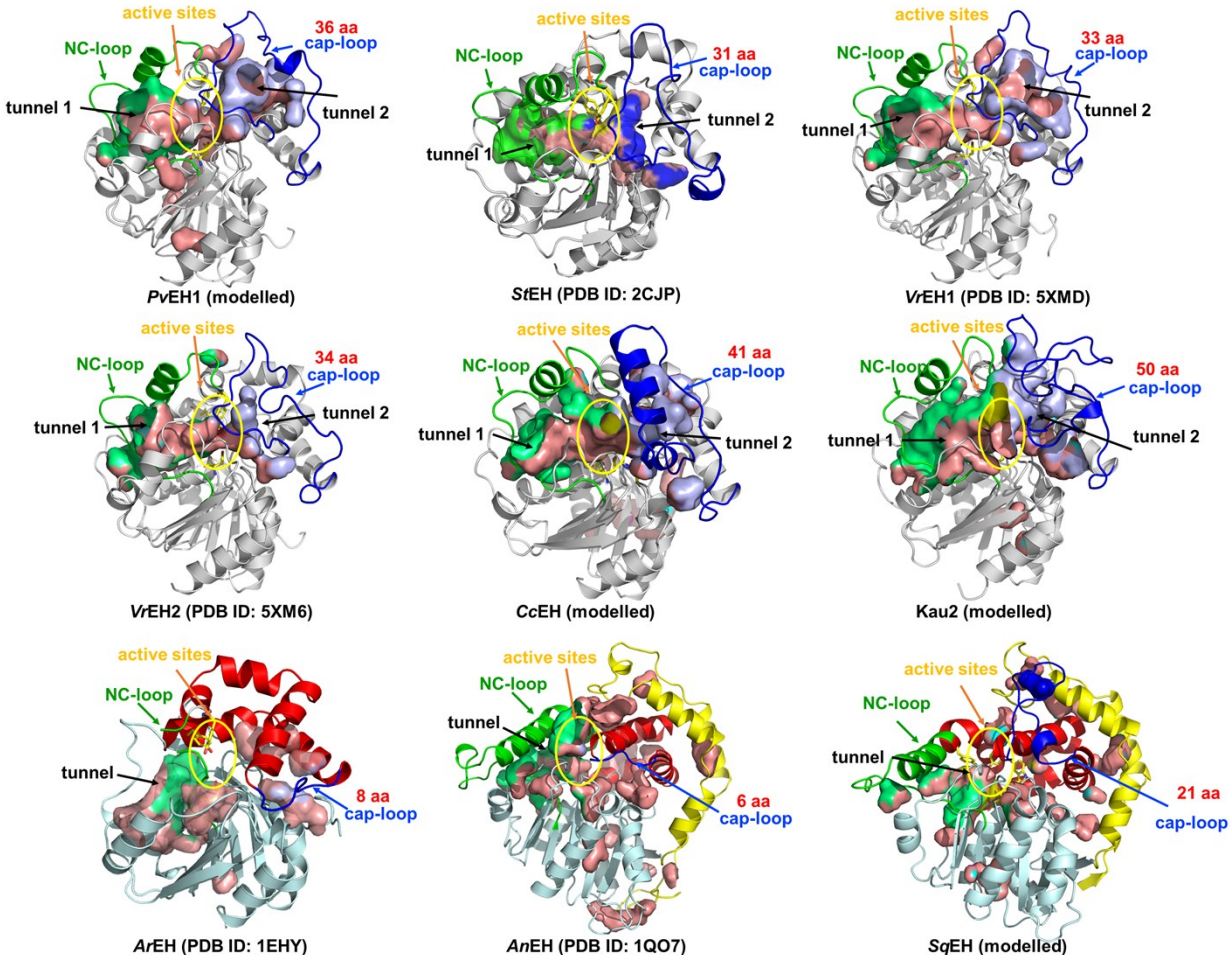

Fig. S8. Compared with the 3-D structures of reported EHs. *Pv*EH1 (*Phaseolus vulgaris* EH, GenBank: AKJ75509, modelled based on *Vr*EH1, this study), *St*EH (*Solanum tuberosum* EH, GenBank: NP_001275417),[19] *Vr*EH1 (*Vigna radiata* EH, GenBank: ADP68585),[17] VrEH2 (*Vigna radiata* EH, GenBank: AIJ27456),[13,20] *Cc*EH (*Caulobacter crescentus* EH, GenBank: AAK23211, modelled based on MtEHA PDB ID: 5CW2, 48.86% identity)[10], Kau2 (metagenome-derived EH, GenBank: ACO95125, modelled based on MtEHA PDB ID: 5CW2, 44.22% identity),[12,18] *Ar*EH (*Agrobacterium radiobacter* AD1 EH, GenBank: CAA73331),[21] *An*EH (*Aspergillus niger* EH. GenBank: CAB59812)[22] and *Sq*EH (*Sphingomonas* sp. HXN-200 EH, GenBank: ANJ44372).[23] Among them, *Pv*EH1, *St*EH, *Vr*EH1, *Vr*EH2, *Cc*EH and Kua2 were reported to display the retention and inversion of configuration via attacking at benzylic carbon (C_α) of one enantiomeric epoxide and terminal carbon (C_β) of another enantiomeric epoxide, while *Ar*EH, *An*EH and *Sq*EH were reported to display the retention of configuration via attacking at terminal carbon (Cβ) of both enantiomeric epoxides. Compared the 3-D structures of reported EHs clearly shows differences in the character of their active sites. The effective loss of the ‘‘inside’’ tunnel 2 in *Ar*EH, *An*EH and *Sq*EH with short cap-loop (6-21 aa) gives rise to its marked preference for attacking terminal carbon (C_β) of epoxides. Differently, the intrinsic shape of SBP in *Pv*EH1, *St*EH, *Vr*EH1, *Vr*EH2, *Cc*EH and Kua2 with long cap-loop (31-50 aa) gives rise to their unique two-tunnel SBP, which substrates can reasonably be expected to bind to each of tunnels to present regiocomplementary toward both enantiomeric epoxides.

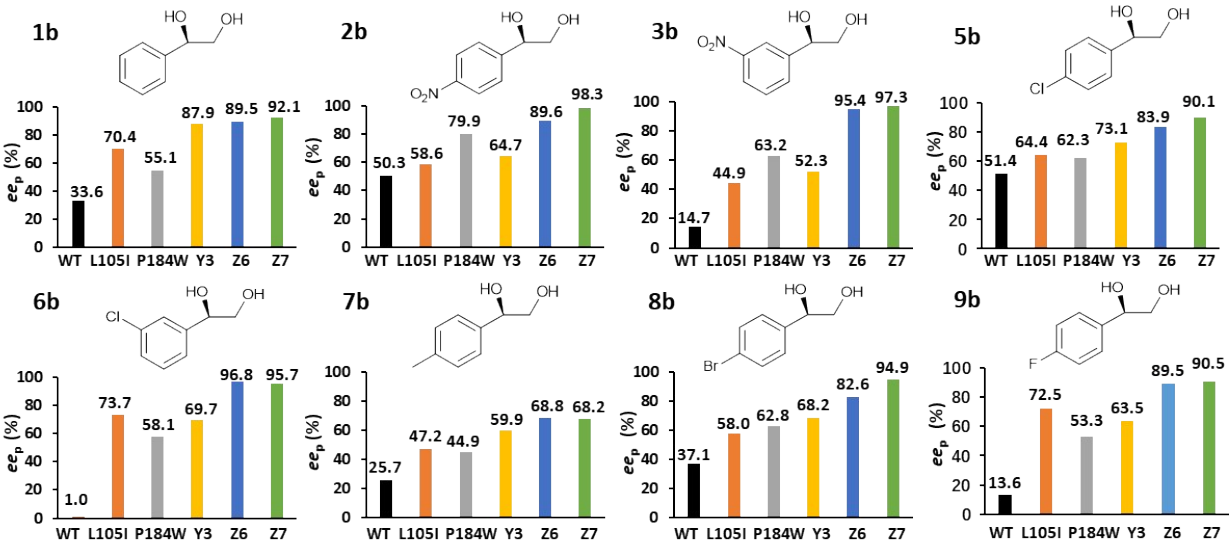

Fig. S9 Enantioconvergence of WT and five mutants toward *rac*- 1a–3a and 5a–9a to access corresponding (*R*)-1,2-diols.

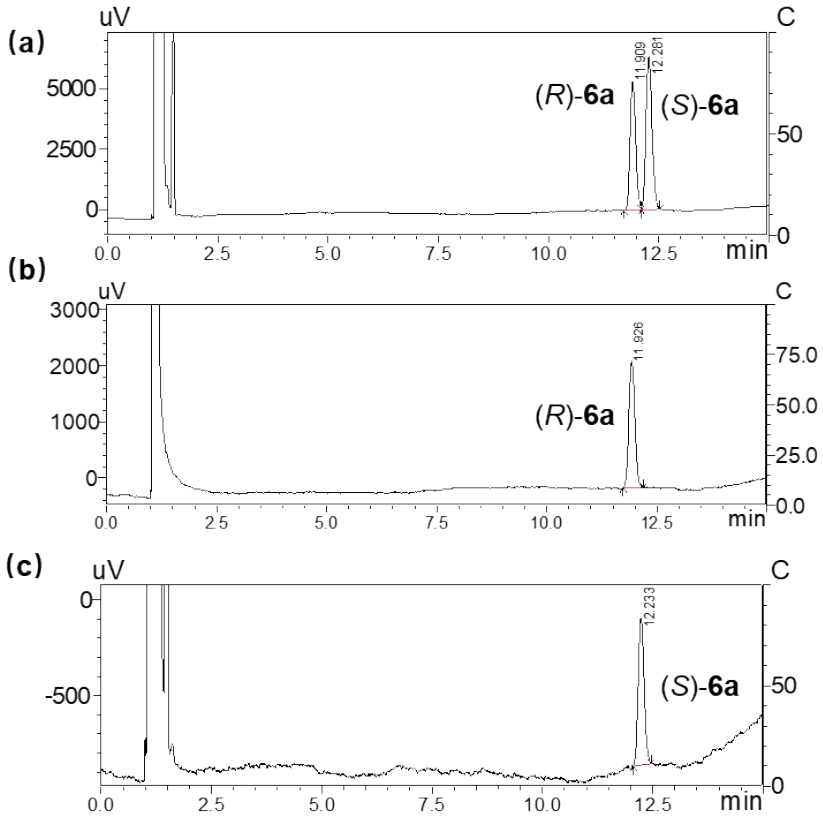

Fig. S10 Chiral GC spectra of *rac*-6a (a), (*R*)-6a (b) and (*S*)-6a (c). Chiral GC column is CP-ChiralSil-DEX CB capillary column (25 m × 0.25 μm, Chrompack, Netherlands). Condition: Carrier gas: N2; 3 ml/min; Split ratio: 50:1; Injector and detector (FID) temperature: 220 ºC; Column temperature: 110 ºC for 14 min. The retention time of (*R*)-**6a** and (*S*)-**6a** are 11.9 and 12.2 min.

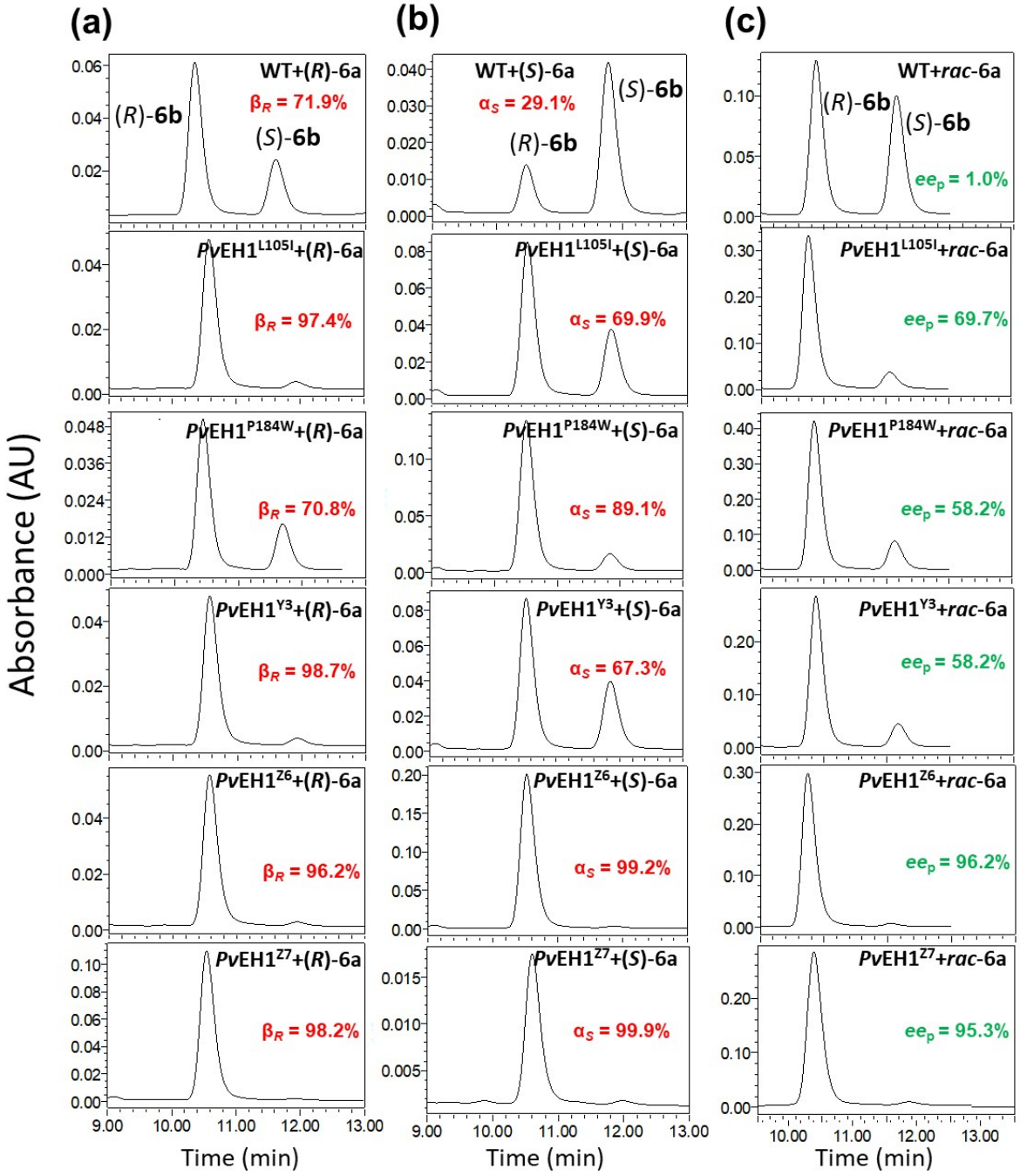

Fig. S11 Chiral HPLC spectra for the hydrolysis of (*R*)-6a (a), (*S*)-6a (b) and *rac*-6a (c) catalysed by WT and mutants. The retention times of (*R*)-6b and (*S*)-6b are 10.5 and 11.8 min. Regioselectivity coefficients (α_S and β_R) were calculated according to equation: α_S or $\beta_R = R / (R + S) \times 100\%$, where *R* and *S* are product peak areas of (*R*)-**6b** and (*S*)-**6b** using **(*S*)-6a** or **(*R*)-6a** as substrate, respectively. The ee_p was calculated according to equations: $ee_p = (R - S)/ (R + S) \times 100\%$, where *R* and *S* are product peak areas of (*R*)-**6b** and (*S*)-**6b** using ***rac*-6a as substrates.**

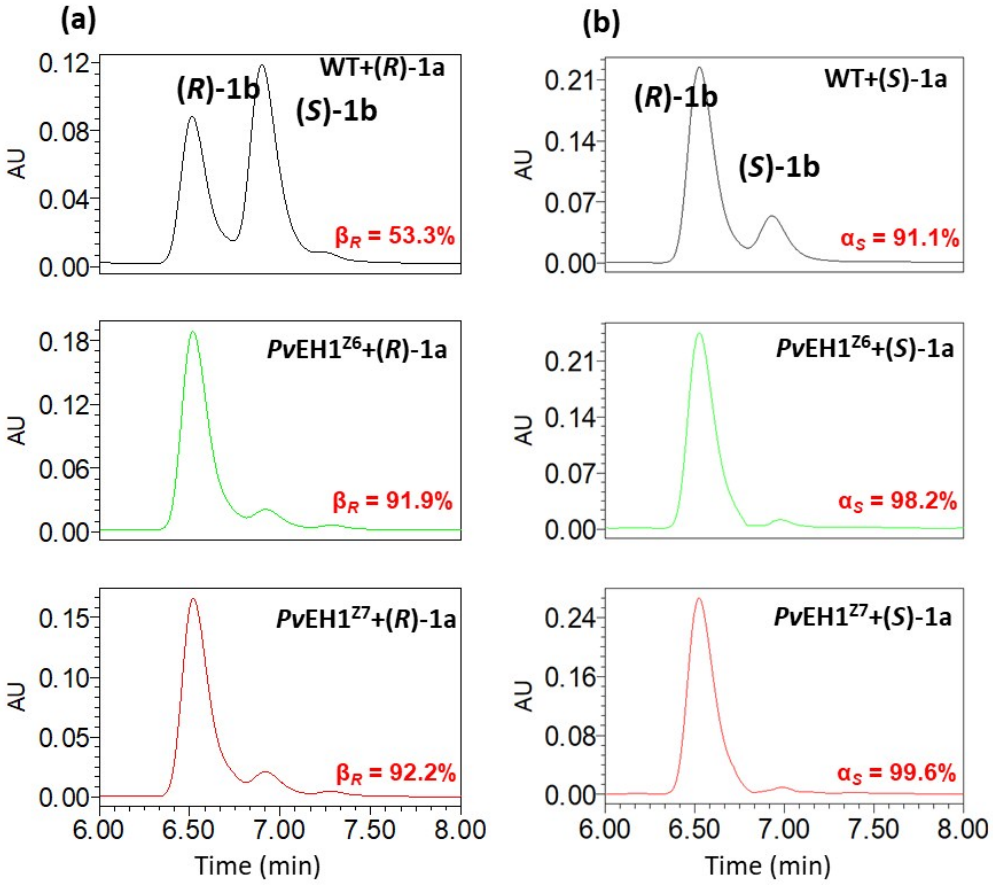

Fig. S12 Chiral HPLC spectra for the hydrolysis of (*R*)-1a (a) and (*S*)-1a (b) catalysed by WT, *Pv*EH^{Z6} and *Pv*EH^{Z7}. The retention times of (*R*)-**1b** and (*S*)-**1b** are 6.51 and 6.90 min. Regioselectivity coefficients (α_S and β_R) were calculated according to equation: α_S or $\beta_R = R / (R + S) \times 100\%$, where *R* and *S* are product peak areas of (*R*)-**1b** and (*S*)-**1b** using **(*S*)-1a** or **(*R*)-1a** as substrate, respectively.

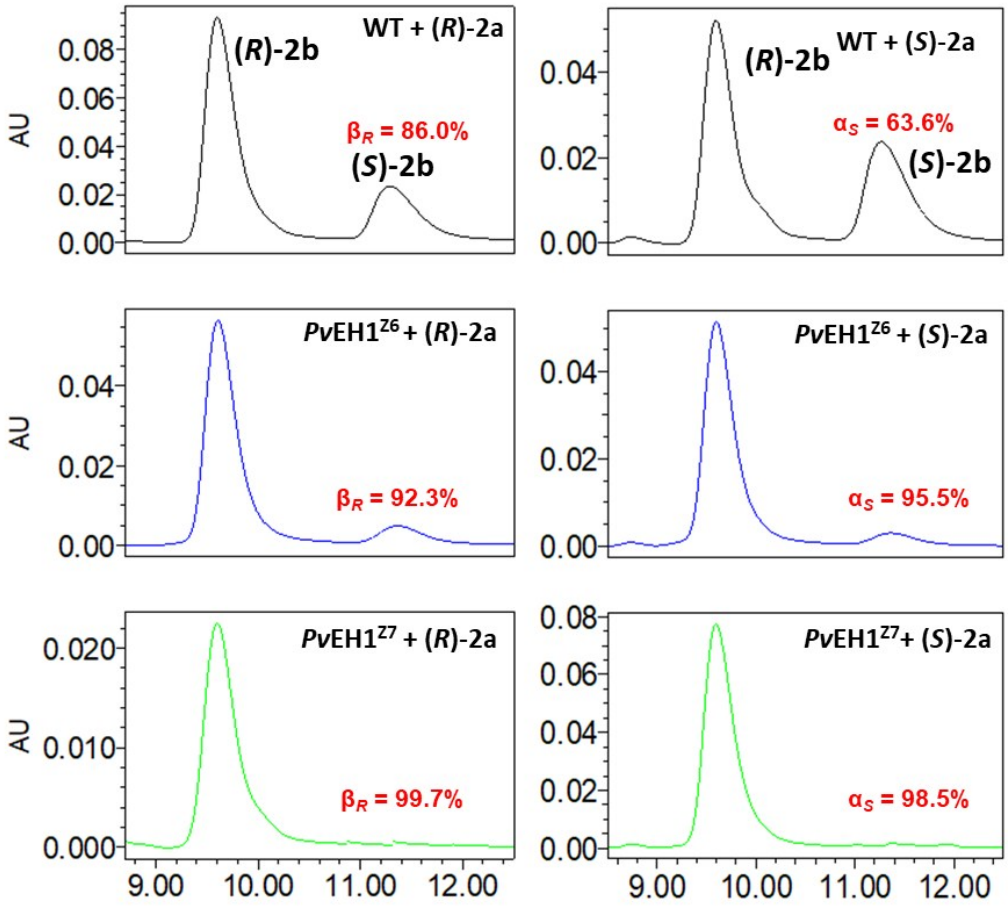

Fig. S13 Chiral HPLC spectra for the hydrolysis of (*R*)-2a (a) and (*S*)-2a (b) catalysed by WT, *Pv*EH^{Z6} and *Pv*EH^{Z7}. Regioselectivity coefficients (α_S and β_R) were calculated according to equation: α_S or $\beta_R = R / (R + S) \times 100\%$, where *R* and *S* are product peak areas of (*R*)-**2b** and (*S*)-**2b** using **(*S*)-2a** or **(*R*)-2a** as substrate, respectively.

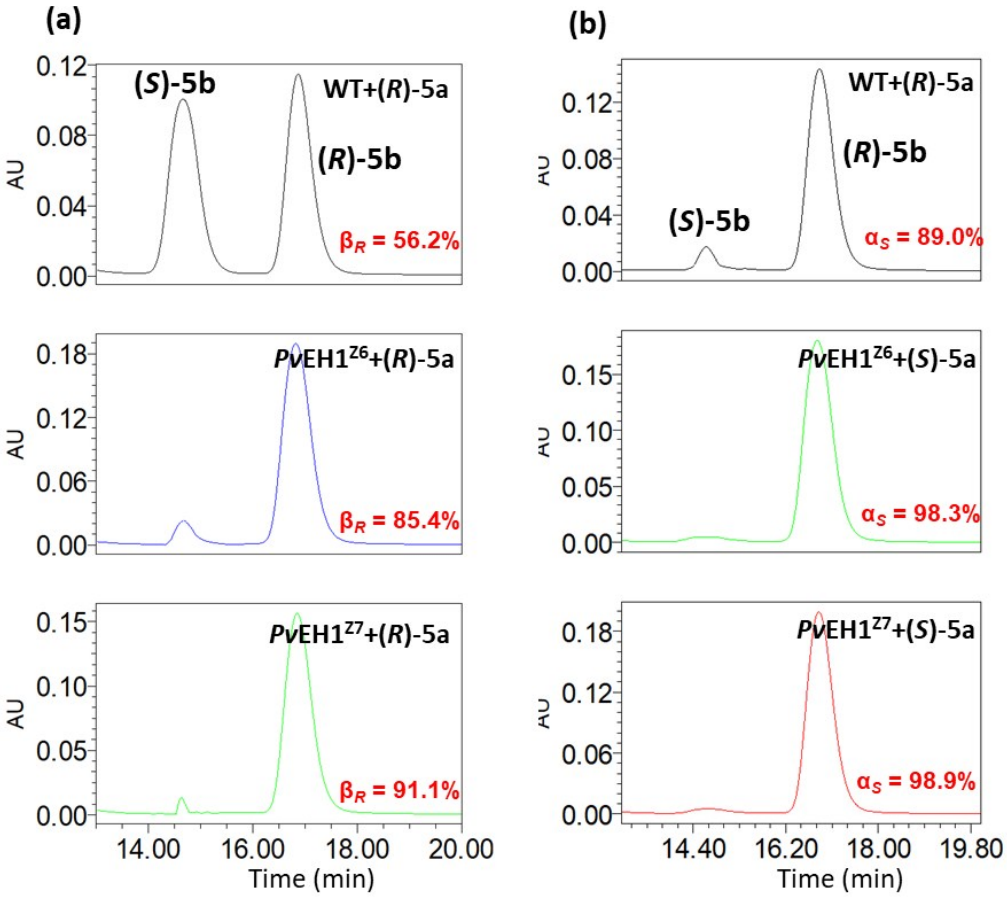

Fig. S14 Chiral HPLC spectra for the hydrolysis of (*R*)-5a (a) and (*S*)-5a (b) catalysed by WT, *Pv*EH^{Z6} and *Pv*EH^{Z7}. Regioselectivity coefficients (α_S and β_R) were calculated according to equation: α_S or $\beta_R = R / (R + S) \times 100\%$, where R and S are product peak areas of (*R*)-**5b** and (*S*)-**5b** using **(*S*)-5a** or **(*R*)-5a** as substrate, respectively.

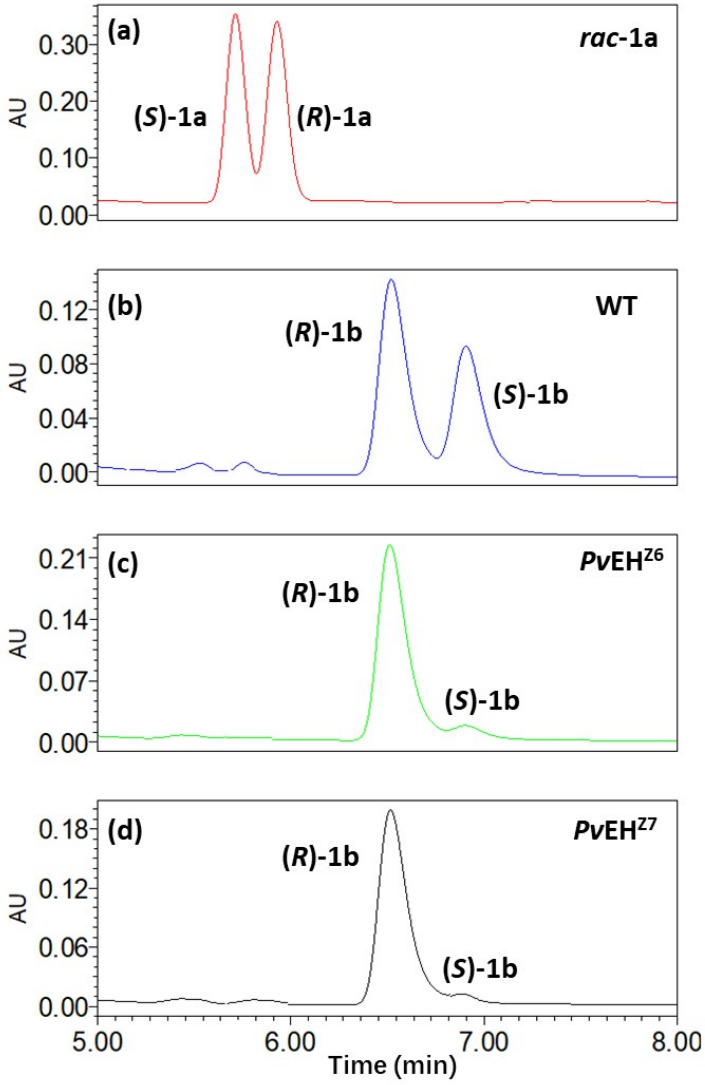

Fig. S15 Chiral HPLC spectra for the enantioconvergent hydrolysis of *rac*-1a (a) by WT (b), *Pv*EH^{Z6} (c) and *Pv*EH^{Z7} (d).

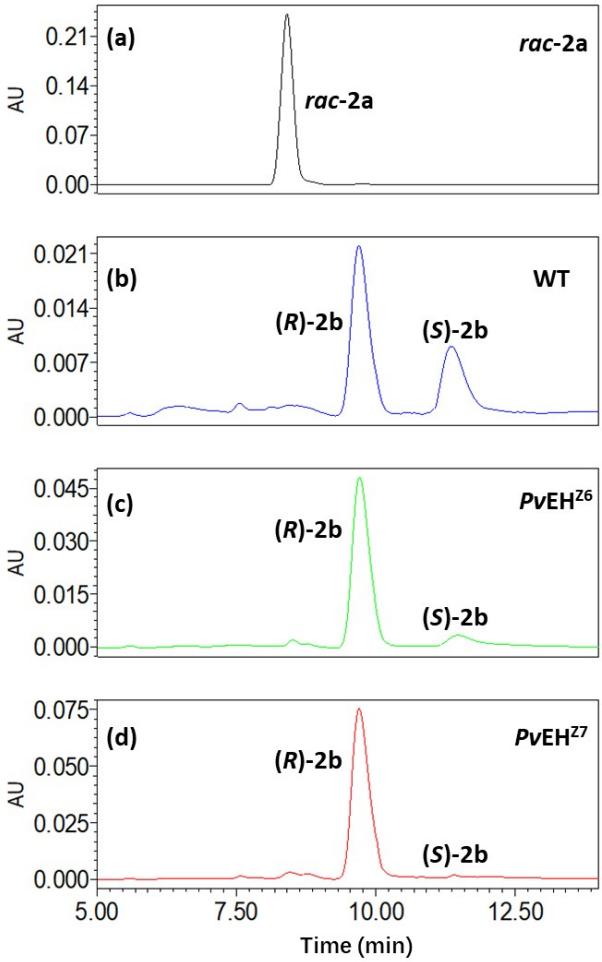

Fig. S16 Chiral HPLC spectra for the enantioconvergent hydrolysis of *rac*-2a (a) by WT (b), *Pv*EH^{Z6} (c) and *Pv*EH^{Z7} (d).

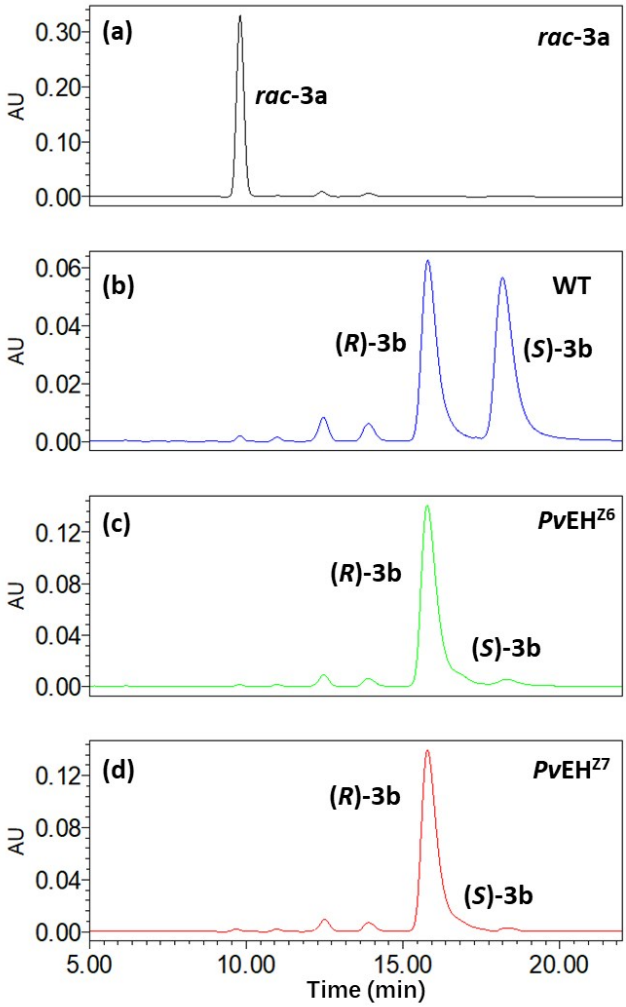

Fig. S17 Chiral HPLC spectra for the enantioconvergent hydrolysis of *rac*-3a (a) by WT (b), *Pv*EH^{Z6} (c) and *Pv*EH^{Z7} (d).

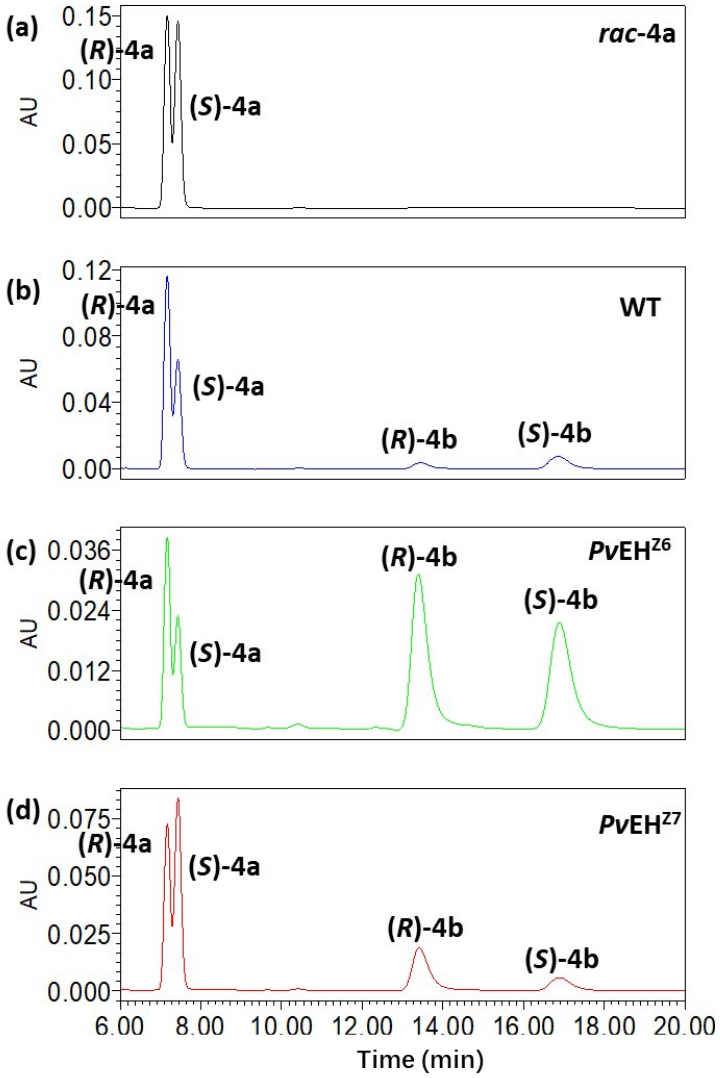

Fig. S18 Chiral HPLC spectra for the enantioconvergent hydrolysis of *rac*-4a (a) by WT (b), *Pv*EH^{Z6} (c) and *Pv*EH^{Z7} (d).

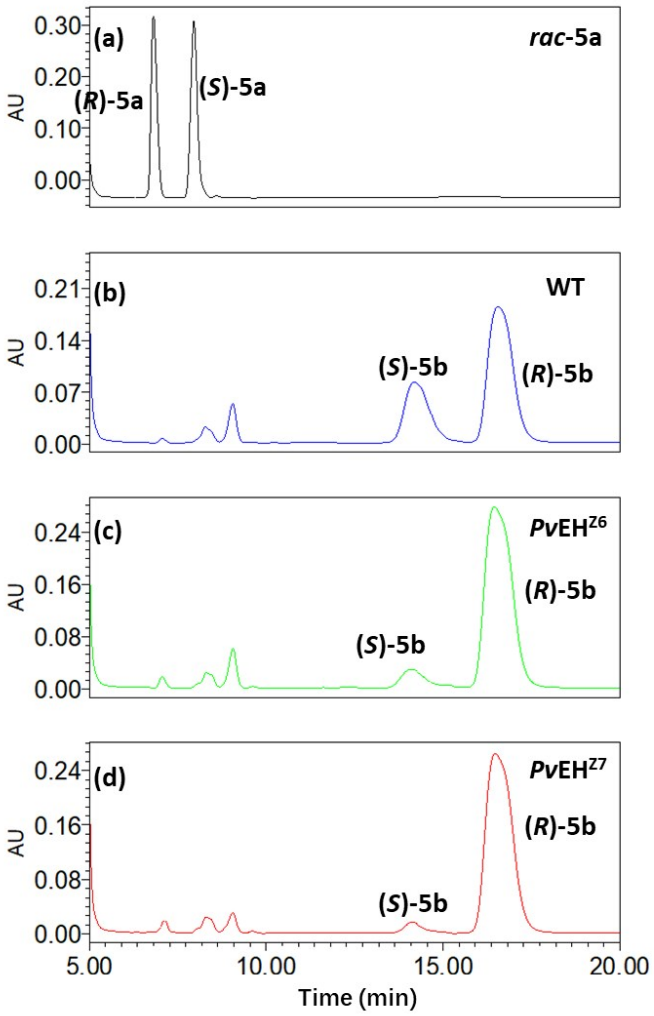

Fig. S19 Chiral HPLC spectra for the enantioconvergent hydrolysis of *rac*-5a (a) by WT (b), *Pv*EH^{Z6} (c) and *Pv*EH^{Z7} (d).

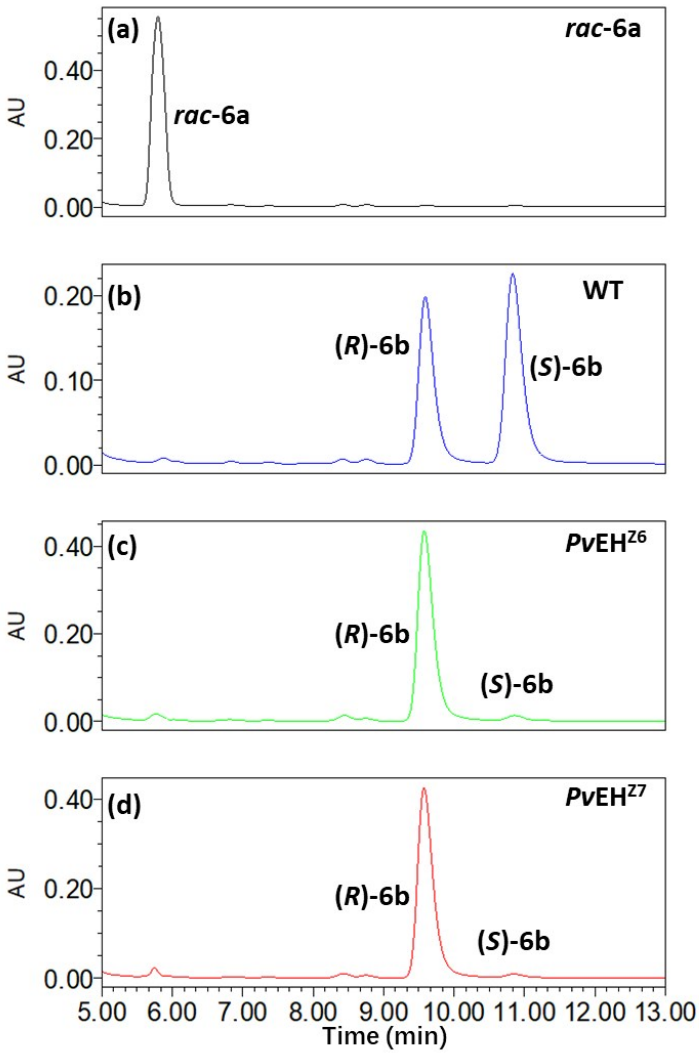

Fig. S20 Chiral HPLC spectra for the enantioconvergent hydrolysis of *rac*-6a (a) by WT (b), *Pv*EH^{Z6} (c) and *Pv*EH^{Z7} (d).

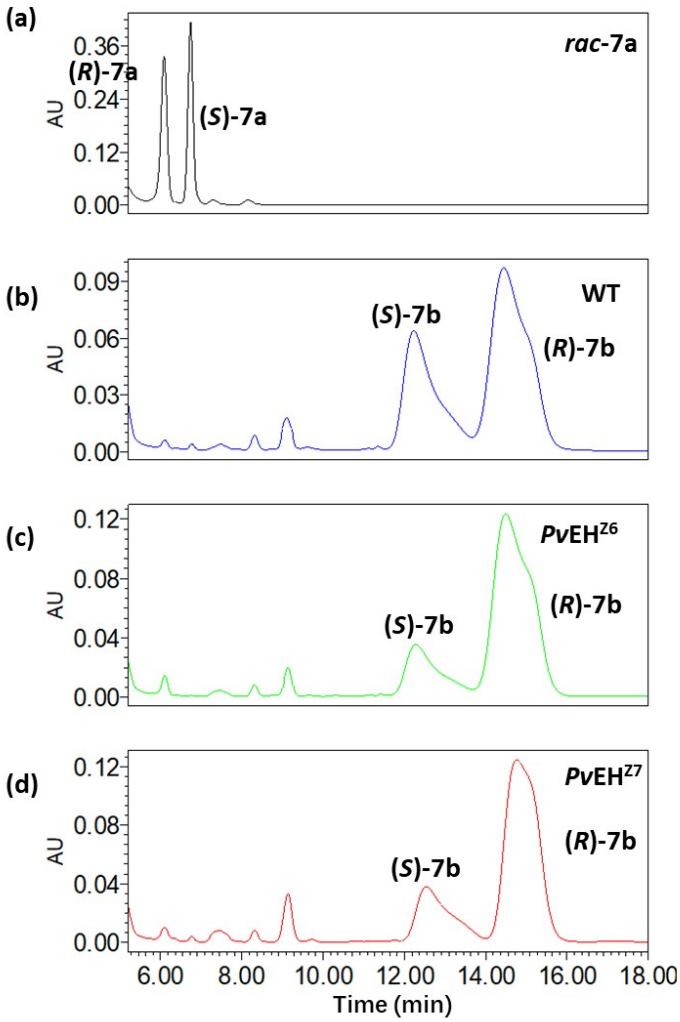

Fig. S21 Chiral HPLC spectra for the enantioconvergent hydrolysis of *rac*-7a (a) by WT (b), *Pv*EH^{Z6} (c) and *Pv*EH^{Z7} (d).

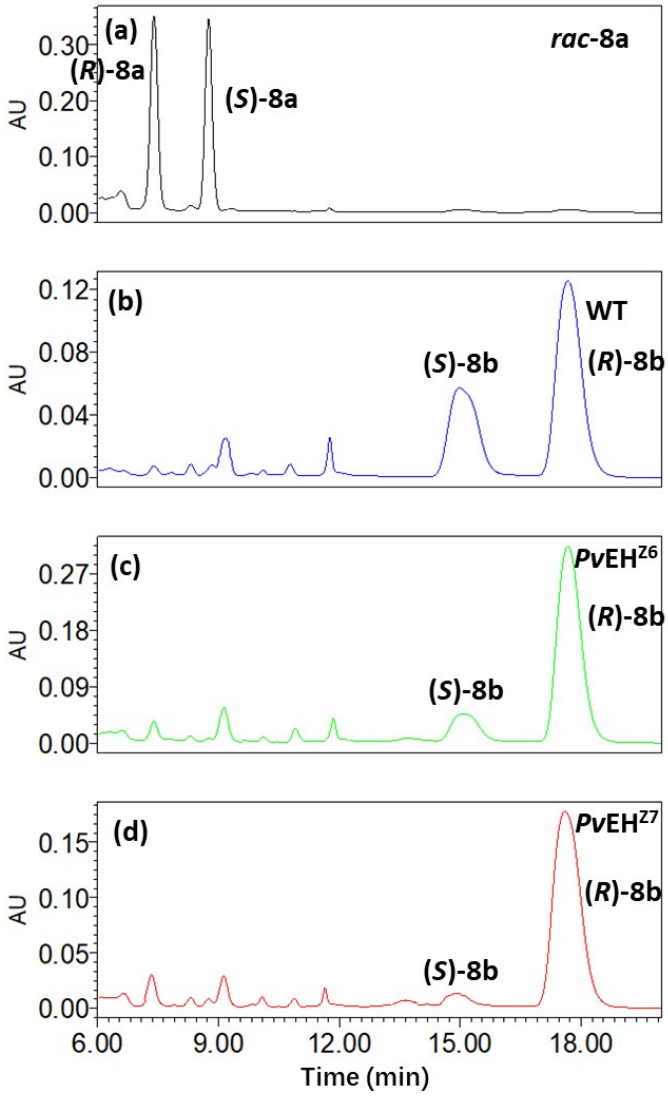

Fig. S22 Chiral HPLC spectra for the enantioconvergent hydrolysis of *rac*-8a (a) by WT (b), *Pv*EH^{Z6} (c) and *Pv*EH^{Z7} (d).

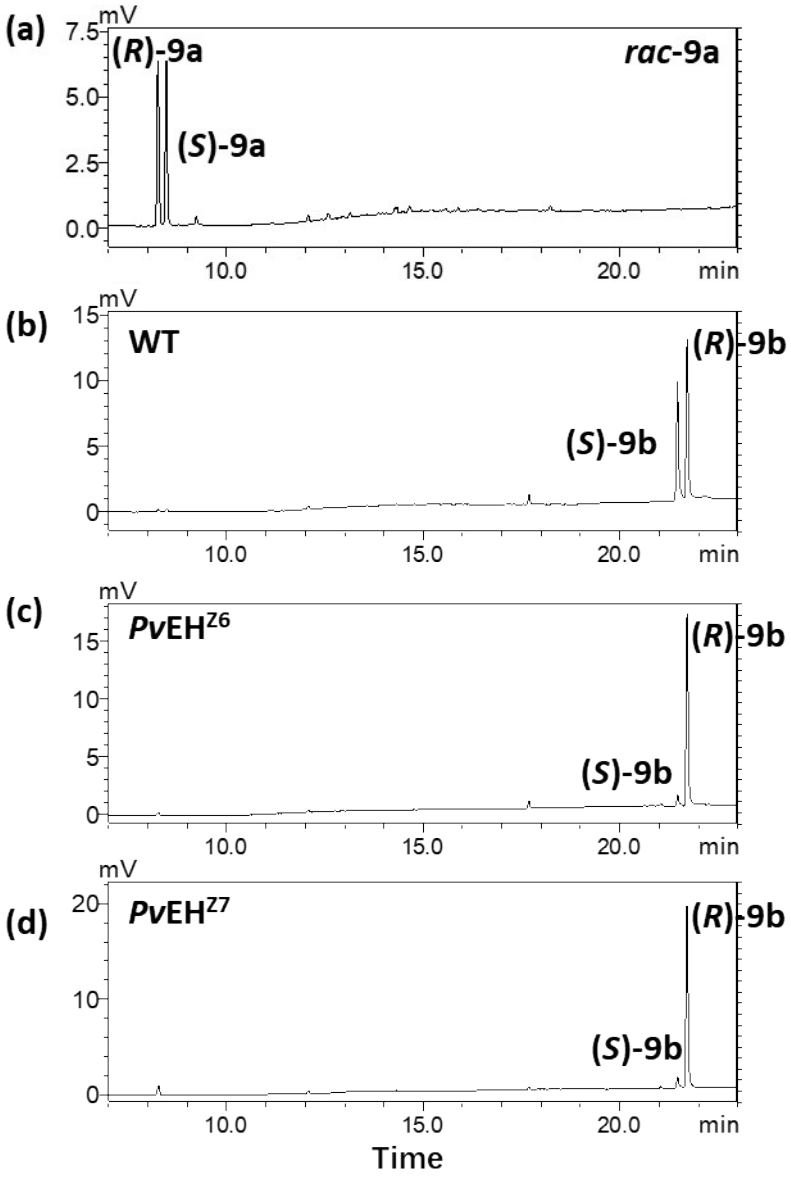

Fig. S23 Chiral GC spectra for the enantioconvergent hydrolysis of *rac*-9a (a) by WT (b), *Pv*EH^{Z6} (c) and *Pv*EH^{Z7} (d).

2.3 ^{1}H NMR spectra of *rac*-epoxides

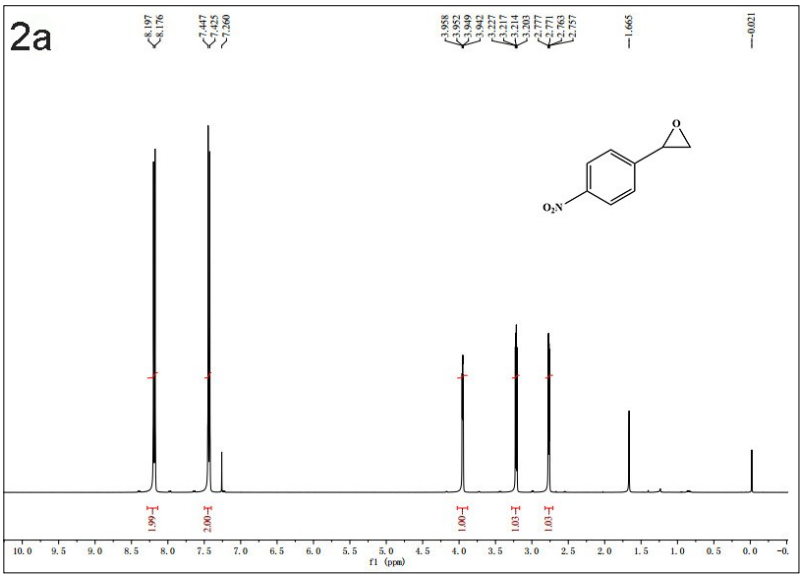

Racemic *p*-nitrostyrene oxide 2a: light yellow solid, purity > 99% (HPLC), ^{1}H NMR (400 MHz, $CDCl_3$, TMS): δ 2.78-2.80 (m, 1H); 3.22-3.25 (m, 1H); 3.96-3.98 (m, 1H); 7.46 (d, $2H_{ar}$, J = 8.8 Hz); 8.21 (d, $2H_{ar}$, J = 8.8 Hz).

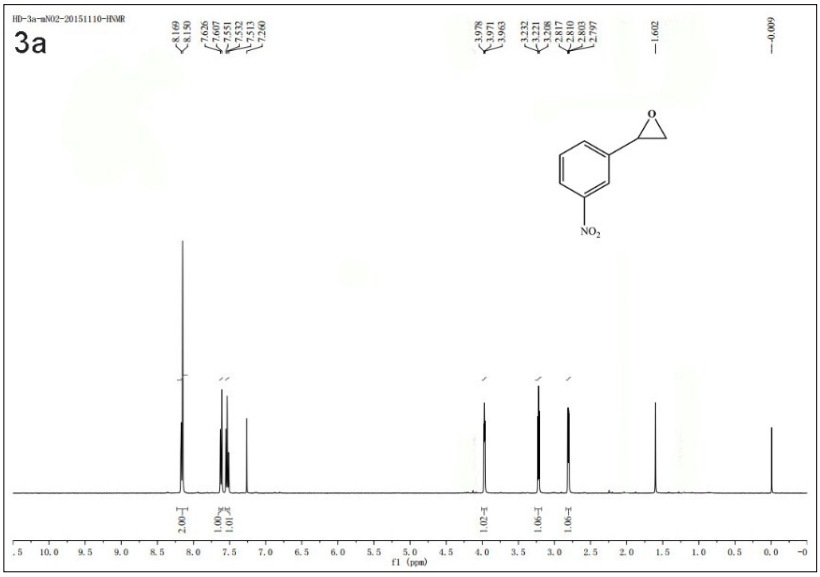

Racemic *m*-nitrostyrene oxide 3a: brown solid, purity > 99% (HPLC), ^{1}H NMR (400 MHz, $CDCl_3$, TMS): δ 8.15-8.17 (m, 2H), 7.60-7.62 (m, 1H), 7.53 (t, 1H, J =7. 6Hz), 3.97 (t, 1H, J = 3.0 Hz), 3.23 (t, 1H, J =4.8 Hz), 2.81 (dd, 1H, J_1 = 2.8 Hz, J_2 = 5.6 Hz)

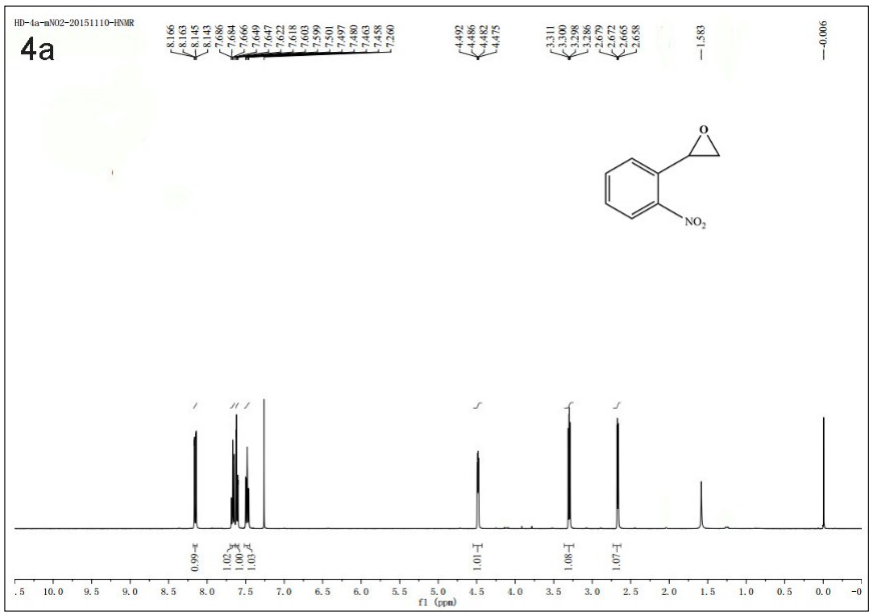

Racemic *o*-nitrostyrene oxide 4a: brown yellow solid, purity > 98% (HPLC). ^{1}H NMR (400 MHz, $CDCl_3$, TMS): δ 8.16 (d, J = 8.0 Hz, 1H), 7.68 (t, J = 8.0 Hz, 1H), 7.62 (d, J = 7.6 Hz, 1H), 7.50 (t, J = 7.6 Hz, 1H), 4.49 (q, J = 2.4 Hz, 1H), 3.31 (t, J = 5.2 Hz, 1H), 2.67 (dd, J_1 = 2.8 Hz, J_2 = 5.6 Hz, 1H)

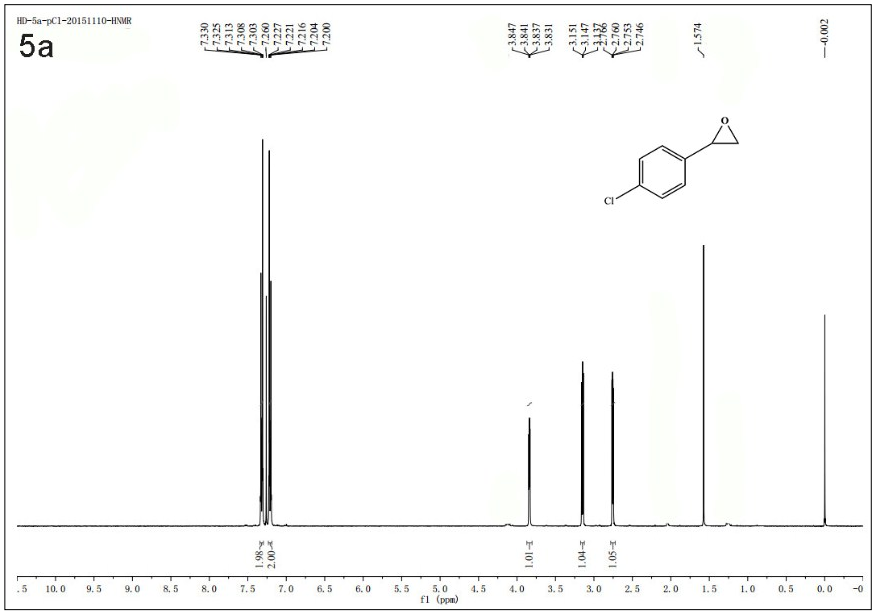

Racemic *p*-chlorostyrene oxide 5a: light yellow oil, purity > 99% (HPLC), ^{1}H NMR (400 MHz, $CDCl_3$, TMS): δ 7.33 (d, J = 8.8 Hz, 2H), 7.22 (d, J = 8.4 Hz, 2H), 3.84 (q, J_1 = 2.4 Hz, J_2 = 4. 0Hz, 1H), 3.16 (dd, J_1 = 4.0 Hz, J_2 = 5.6 Hz, 1H), 2.76 (dd, J_1 = 2.4 Hz, J_2 = 5.6 Hz, 1H)

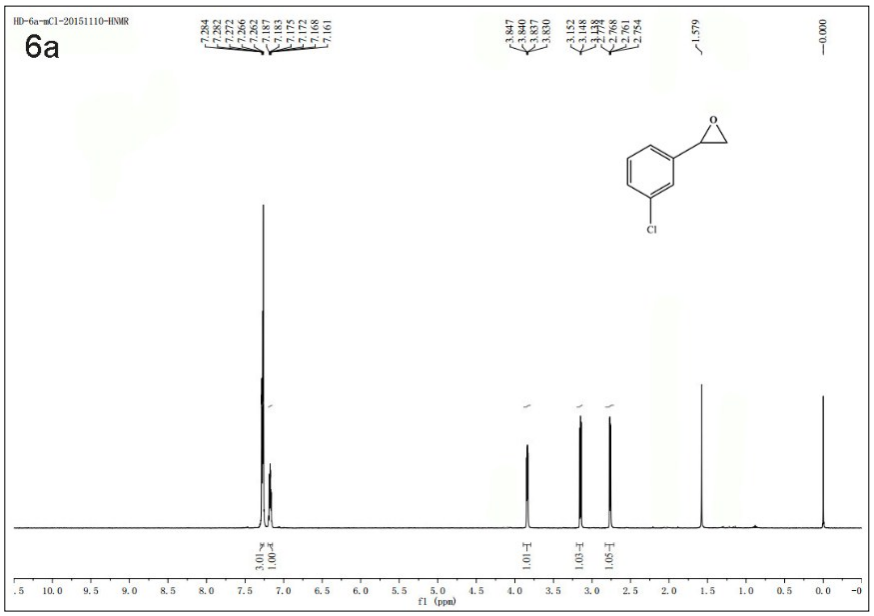

Racemic *m*-chlorostyrene oxide 6a: pale yellow oil, purity > 98% (HPLC), ^{1}H NMR (400 MHz, $CDCl_3$, TMS): δ 7.26-7.2 (m, 3H), 7.16-7.18 (m, 1H), 3.84 (dd, J_1 = 2.8 Hz, J_2=4.0 Hz, 1H), 3.16 (dd, J_1 = 4.0 Hz, J_2 = 5.6 Hz, 1H), 2.77 (dd, J_1=2.4 Hz, J_2=5.6 Hz, 1H)

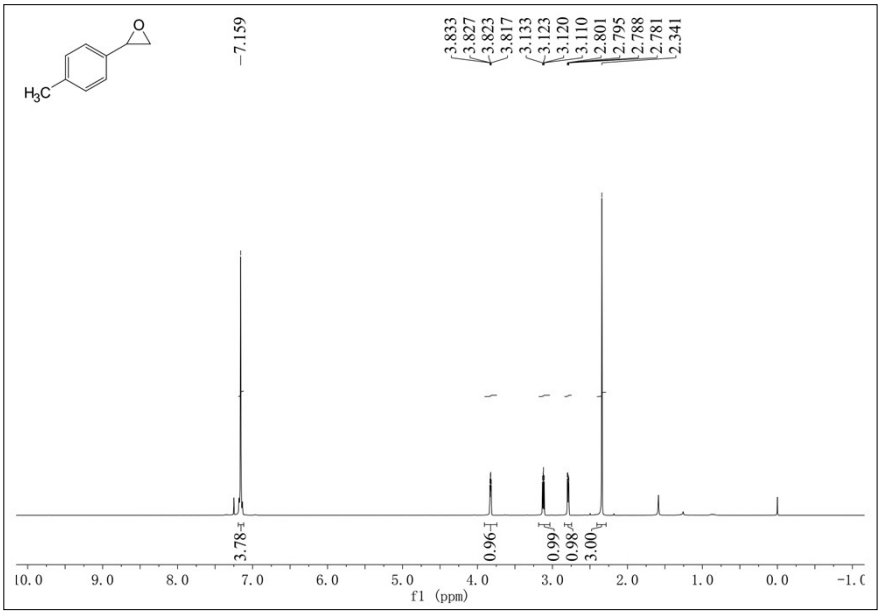

Racemic *p*-methylstyrene oxide 7a: colorless oil, ^{1}H NMR (400 MHz, $CDCl_3$, TMS): δ 7.16 (s, 4H), 3.83 (q, J_1 = 4.0 Hz, $J2$ = 4.0 Hz, 1H), 3.12 (q, J_1 = 5.2 Hz, J_2 = 5.2 Hz, 1H), 2.79 (dd, J_1 = 2.4 Hz, J_2 = 3.2 Hz, 1H), 2.34 (s, 4H).

2.4 ^{1}H NMR spectra of (*R*)-1,2-diols

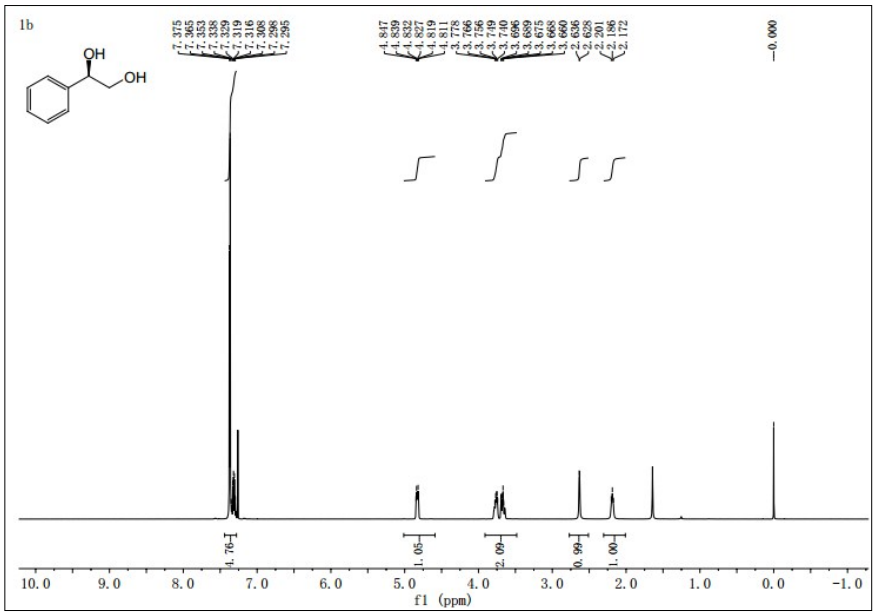

(*R*)-phenylethane-1,2-diol 1b: 90.3% ee_p. ^{1}H NMR (400 MHz, $CDCl_3$, TMS): δ 7.30–7.37 (m, 5H), 4.81–4.85 (m, 1H), 3.66–3.78 (m, 2H), 2.64 (d, J = 3.2 Hz, 1H), 2.19 (t, J = 11.6 Hz, 1H).

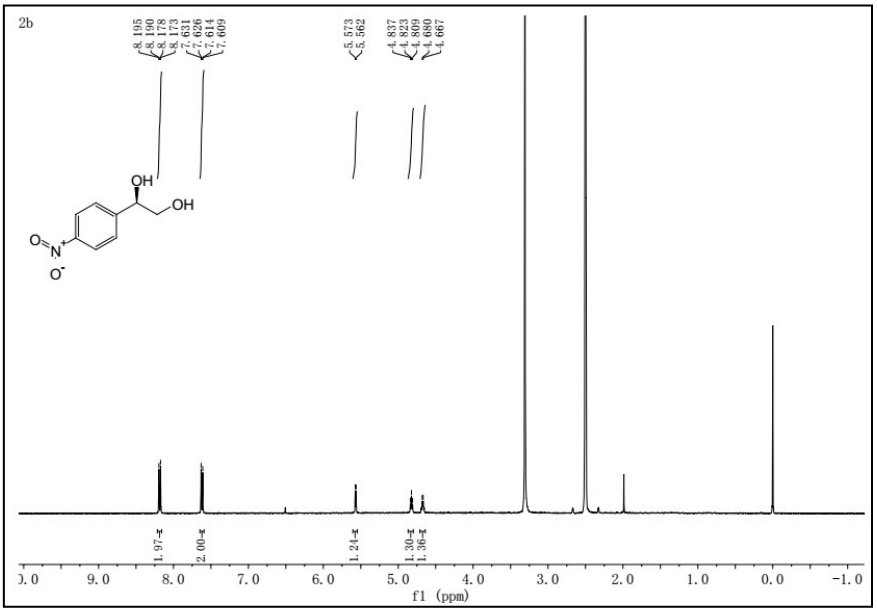

(*R*)-*p*-nitrophenylethane-1,2-diol 2b: 86.7% ee_p.^{1}H NMR (400 MHz, DMSO, TMS): δ 8.20–8.17 (m, 2H), 7.61–7.63 (m, 2H), 5.57 (d, J = 4.4 Hz, 1H), 4.82 (t, J = 11.2 Hz, 1H), 4.67 (dd, J_1 = 10.0 Hz, J_2 = 10.8 Hz, 1H)

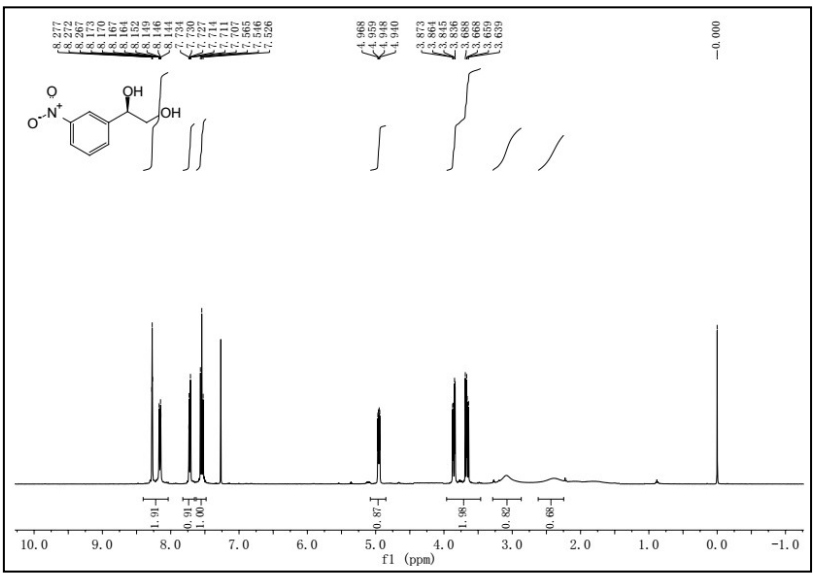

(*R*)-*m*-nitrophenylethane-1,2-diol 3b: 95.1% ee_p. ^{1}H NMR (400 MHz, $CDCl_3$, TMS): δ 8.14–8.28 (m, 2H), 7.72 (d, J = 7.6 Hz, 1H), 7.55 (t, J = 15.6 Hz, 1H), 4.95 (dd, J_1 = 8.0 Hz, J_2 = 7.7 Hz, 1H), 3.64–3.87 (m, 2H), 3.08 (s, 1H), 2.39 (s, 1H).

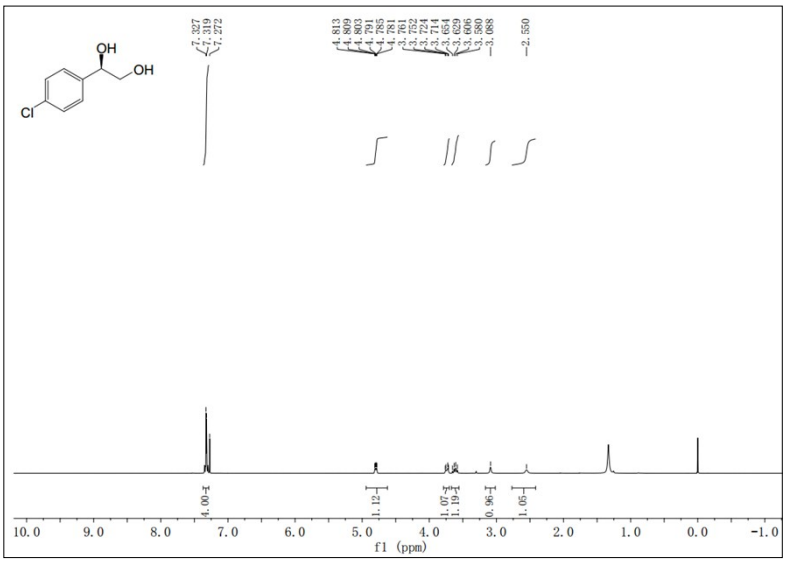

(*R*)-*p*-chlorophenylethane-1,2-diol 5b: 83.5% ee_p. ^{1}H NMR (400 MHz, $CDCl_3$, TMS): δ 7.30–7.35 (m, 4H), 4.78–4.81 (m, 1H), 3.76–3.71 (m, 1H), 3.62 (dd, J_1 = 19.2 Hz, J_2 = 19.6 Hz, 1H), 3.09 (s, 1H), 2.55 (s, 1H).

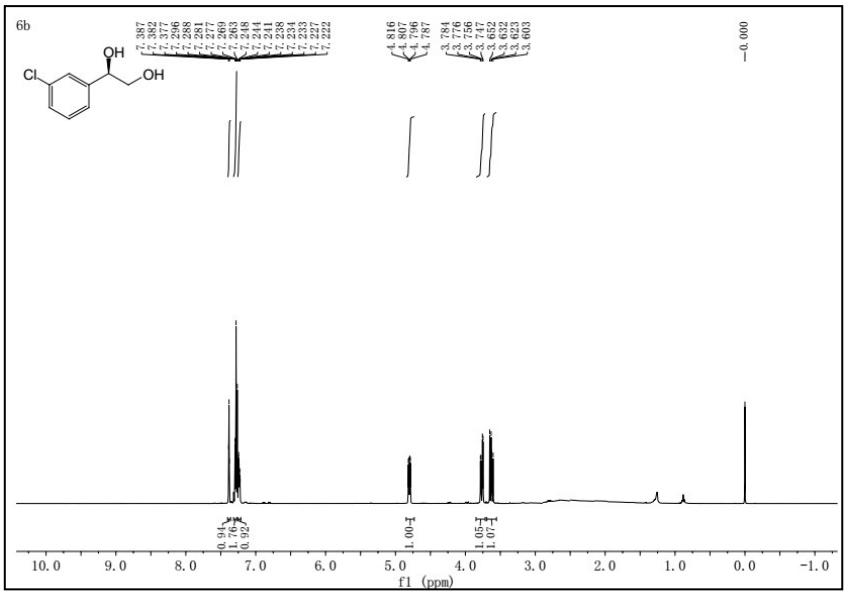

(*R*)-*m*-chlorophenylethane-1,2-diol 6b: 95.6% ee_p. ^{1}H NMR (400 MHz, $CDCl_3$, TMS): δ 7.22–7.39 (m, 4H), 4.80 (dd, J_1 = 3.6 Hz, J_2 = 3.6 Hz, 1H), 3.77 (dd, J_1 = 3.2 Hz, J_2 = 3.6 Hz, 1H), 3.63 (q, J_1 = 11.6 Hz, J_2 = 11.6 Hz, 1H).

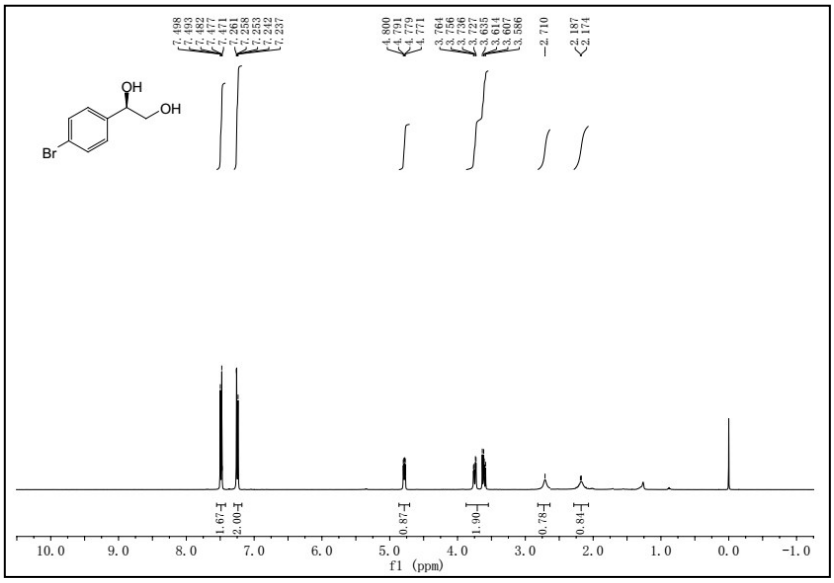

(*R*)-*p*-bromophenylethane-1,2-diol 8b: 80.5% ee_p. ^{1}H NMR (400 MHz, $CDCl_3$, TMS): δ 7.24–7.50 (m, 4H), 4.79 (dd, J_1 = 3.6 Hz, J_2 = 3.2 Hz, 1H), 3.75 (dd, J_1 = 3.2 Hz, J_2 = 3.6 Hz, 1H), 3.61 (q, J_1 = 11.2 Hz, J_2 = 11.2 Hz, 1H), 2.71 (s, 1H), 2.18 (s, 1H).

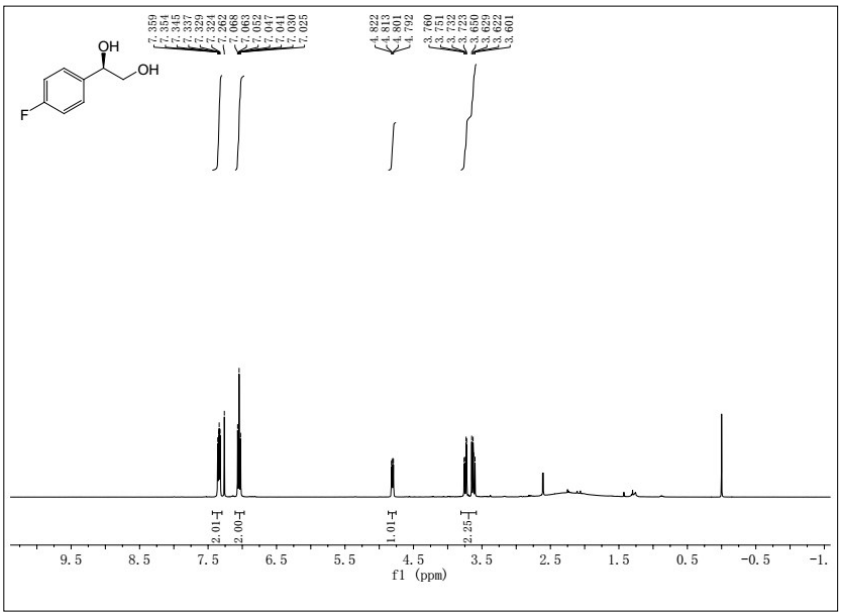

(*R*)-*p*-fluorophenylethane-1,2-diol 9b: 90.6% ee_p.^{1}H NMR (400 MHz, $CDCl_3$, TMS): δ 7.03–7.36 (m, 4H), 4.81 (dd, J_1 = 3.6 Hz, J_2 = 3.6 Hz, 1H), 3.74 (dd, J_1 = 3.6 Hz, J_2 = 3.6 Hz, 1H), 3.63 (q, J_1 = 11.2 Hz, J_2 = 11.2 Hz, 1H).

Reference

1 H. H. Ye, D. Hu, X. L. Shi, M. C. Wu, C. Deng, J. F. Li, *Catal. Commun.,* 2016, **87**, 32.

2 J. Sanchis, L. Fernandez, J. Carballeira, J. Drone, Y. Gumulya, H. Hobenreich, D. Kahakeaw, S. Kille, R. Lohmer, J. Peyralanset al., *Appl. Microbiol. Biot.,* 2008, **81**, 387.

3 Z. T. Sun, R. Lonsdale, X. D. Kong, J. H. Xu, J. H. Zhou, M. T. Reetz, *Angew. Chem. Int. Ed.,* 2015, **54**, 12410.

4 X. D. Kong, Q. Ma, J. H. Zhou, B. B. Zeng, J. H. Xu, *Angew. Chem. Int. Ed.,* 2014, **53**, 6641.

5 C. S. Chen, Y. Fujimoto, G. Girdaukas, C. J. Sih, *J. Am. Chem. Soc.,* 1982, **104**, 7294.

6 M. E. S. Lind, F. Himo, *ACS Catal.,* 2016, **6**, 8145.

7 A. Waterhouse, M. Bertoni, S. Bienert, G. Studer, G. Tauriello, R. Gumienny, F. T. Heer, T. A. P. de Beer, C. Rempfer, L. Bordoliet al., *Nucleic Acids Res.,* 2018, **46**, W296.

8 G. M. Morris, R. Huey, W. Lindstrom, M. F. Sanner, R. K. Belew, D. S. Goodsell, A. J. Olson, *J. Comput. Chem.,* 2009, **30**, 2785.

9 J. Y. Zhou, Y. Wang, G. C. Xu, L. Wu, R. Z. Han, U. Schwaneberg, Y. J. Rao, Y. L. Zhao, J. H. Zhou, Y. Ni, *J. Am. Chem. Soc.,* 2018, **140**, 12645.

10 S. Hwang, C. Y. Choi, E. Y. Lee, *Biotechnol. Lett.,* 2008, **30**, 1219.

11 M. I. Monterde, M. Lombard, A. Archelas, A. Cronin, M. Arand, R. Furstoss, *Tetrahedron Asymmetry,* 2004, **15**, 2801.

12 M. Kotik, V. Stepanek, M. Grulich, P. Kyslik, A. Archelas, *J. Mol. Catal. B: Enzym.,* 2010, **65**, 41.

13 F. L. Li, X. D. Kong, Q. Chen, Y. C. Zheng, Q. Xu, F. F. Chen, L. Q. Fan, G. Q. Lin, J. H. Zhou, H. L. Yuet al., *ACS Catal.,* 2018, **8**, 8314.

14 D. E. Hu, C. D. Tang, C. Li, T. T. Kan, X. L. Shi, L. Feng, M. C. Wu, *J. Agr. Food Chem.,* 2017, **65**, 9862.

15 M. Kotik, A. Archelas, V. Famerova, P. Oubrechtova, V. Kren, *J. Biotechnol.,* 2011, **156**, 1.

16 G. P. Horsman, A. Lechner, Y. Ohnish, B. S. Moore, B. Shen, *Biochemistry,* 2013, **52**, 5217.

17 Q. Q. Zhu, W. H. He, X. D. Kong, L. Q. Fan, J. Zhao, S. X. Li, J. H. Xu, *Appl. Microbiol. Biot.,* 2014, **98**, 207.

18 M. Kotik, W. Zhao, G. Lacazio, A. Archelas, *J. Mol. Catal. B: Enzym.,* 2013, **91**, 44.

19 S. L. Mowbray, L. T. Elfstrom, K. M. Ahlgren, C. E. Andersson, M. Widersten, *Protein Sci.,* 2006, **15**, 1628.

20 Y. W. Wu, X. D. Kong, Q. Q. Zhu, L. Q. Fan, J. H. Xu, *Catal. Commun.,* 2015, **58**, 16.

21 M. Nardini, I. S. Ridder, H. J. Rozeboom, K. H. Kalk, R. Rink, D. B. Janssen, B. W. Dijkstra, *J. Biol. Chem.,* 1999, **274**, 14579.

22 (a) J. Y. Zou, B. M. Hallberg, T. Bergfors, F. Oesch, M. Arand, S. L. Mowbray, T. A. Jones, *Struct. Fold Des.,* 2000, **8**, 111; (b) M. T. Reetz, M. Bocola, L. W. Wang, J. Sanchis, A. Cronin, M. Arand, J. Y. Zou, A. Archelas, A. L. Bottalla, A. Naworytaet al., *J. Am. Chem. Soc.,* 2009, **131**, 7334.

23 S. K. Wu, A. T. Li, Y. S. Chin, Z. Li, *ACS Catal.,* 2013, **3**, 752.